SOLVING THE (NUCLEAR) QUANTUM MANY-BODY PROBLEM WITH NEURAL NETWORKS

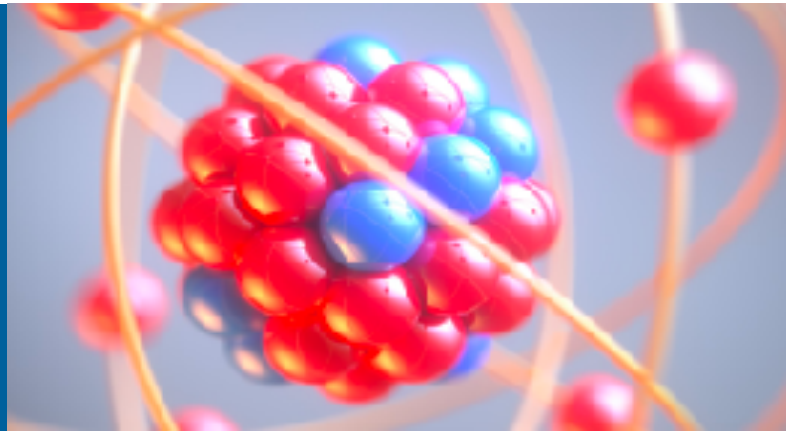

ALESSANDRO LOVATO

TIFPA Trento Institute for Fundamental Physics and Applications

Argonne NATIONAL LABORATORY

Precision Many-Body Physics 2023

June 13, 2023

COLLABORATORS

C. Adams, **B. Fore**

G. Carleo, **G. Pescia**

S. Gandolfi

J. Kim, M. Hjorth-Jensen

N. Rocco

INTRODUCTION

Atomic nuclei are strongly interacting many-body systems exhibiting self-emerging properties including: shell structure, pairing and superfluidity, deformation, and clustering.

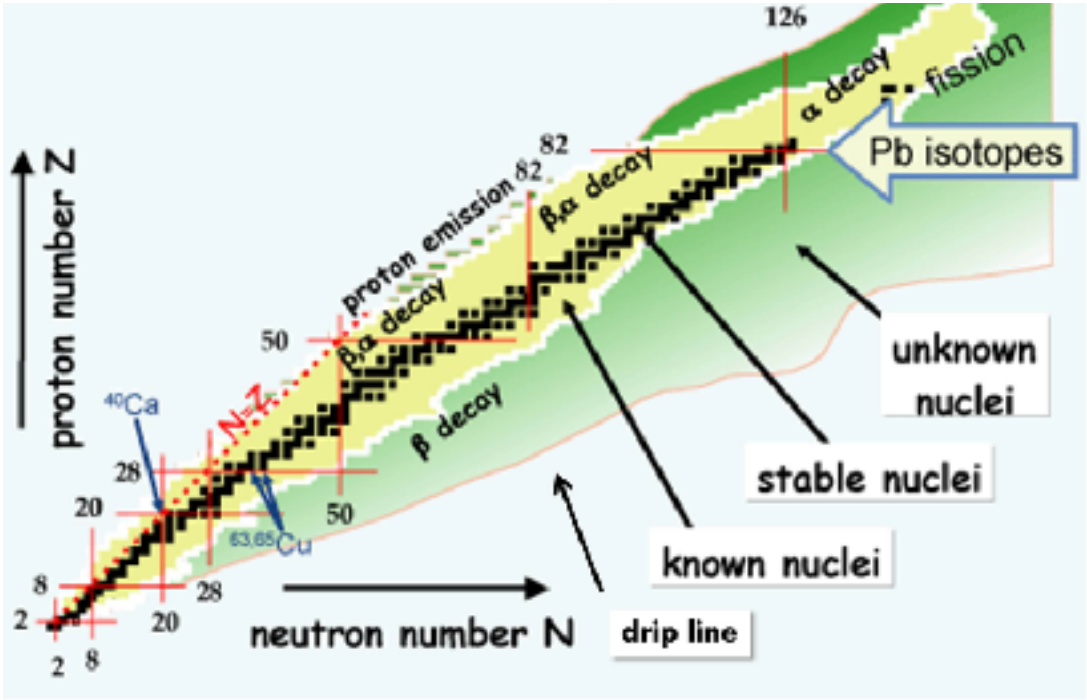

INTRODUCTION

Oscillation parameters are measured by comparing the neutrino flux at near and far detectors

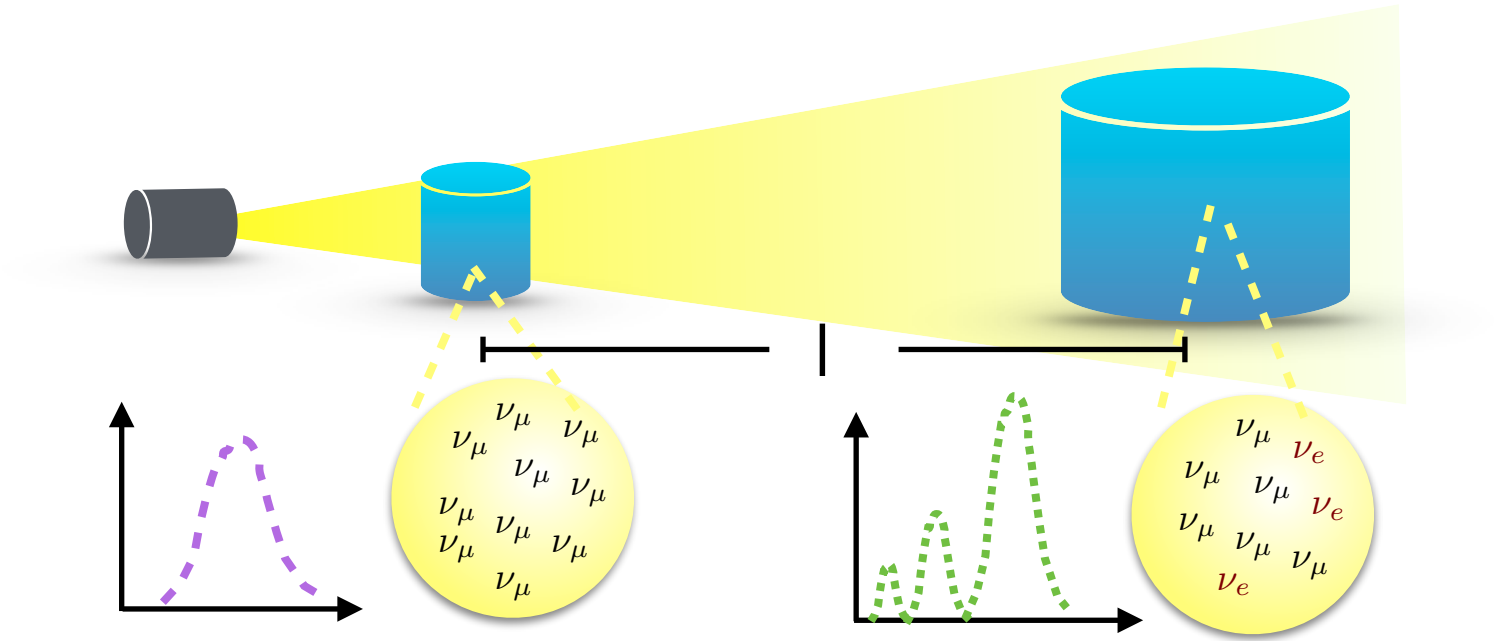

Credit: N. Rocco

INTRODUCTION

Oscillation parameters are measured by comparing the neutrino flux at near and far detectors

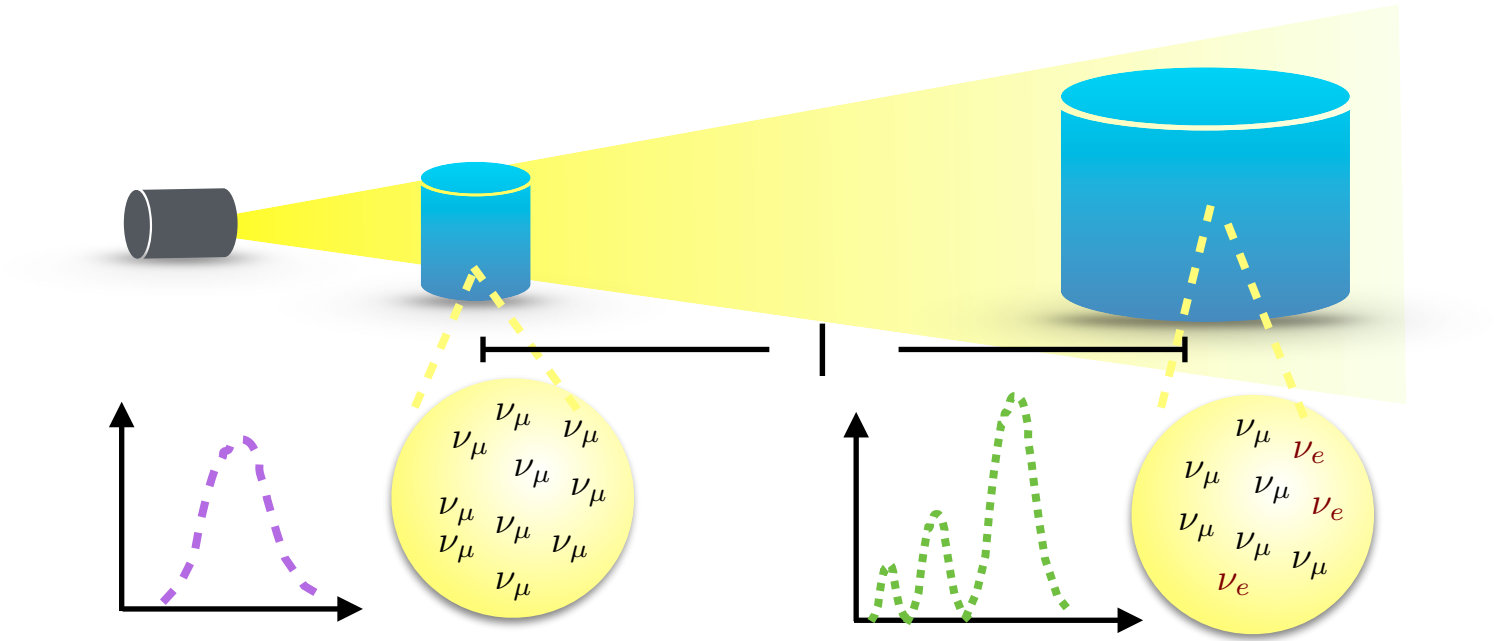

Credit: N. Rocco

INTRODUCTION

Oscillation parameters are measured by comparing the neutrino flux at near and far detectors

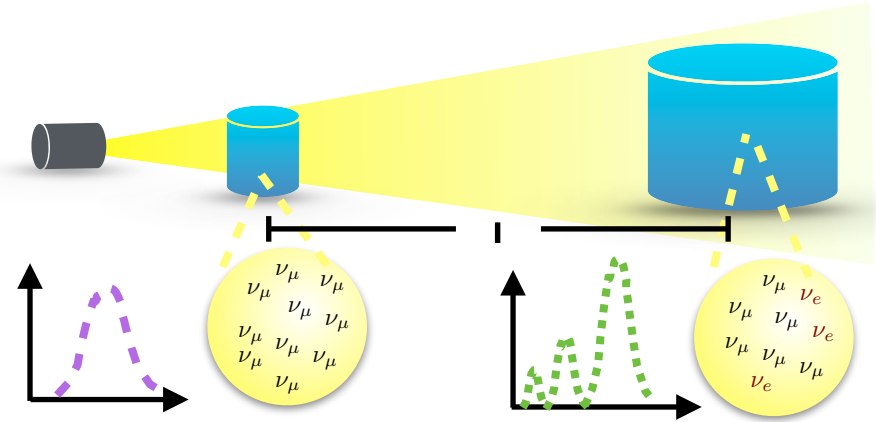

Accurate neutrino-nucleus scattering calculations critical for the success of the experimental program

Credit: N. Rocco

If observed, $0\nu\beta\beta$ would provide key insights into physics beyond the Standard Model

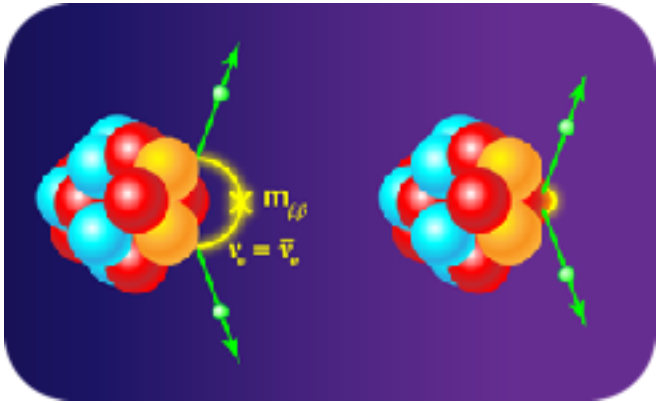

Relating experimental constraints on 0νββ decay rates to the neutrino masses requires quantitative estimates of nuclear matrix elements

INTRODUCTION

An accurate understanding of nuclear dynamics is critical for multi-messenger astronomy

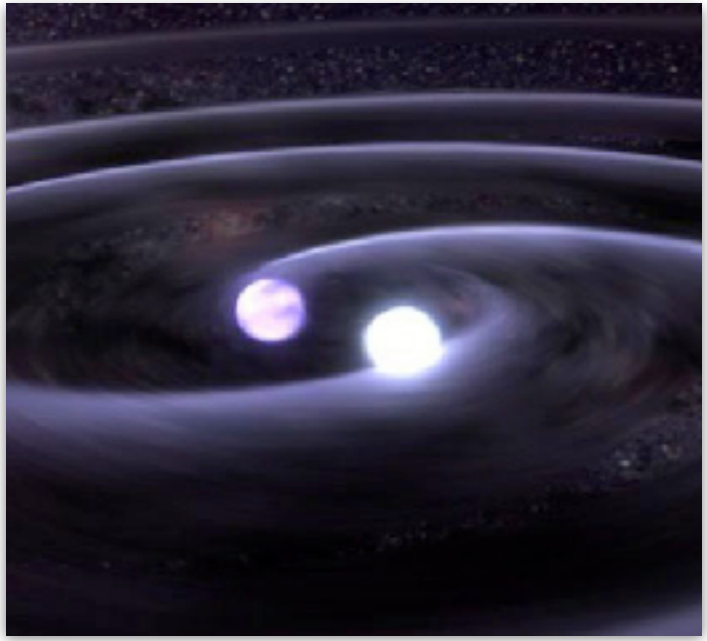

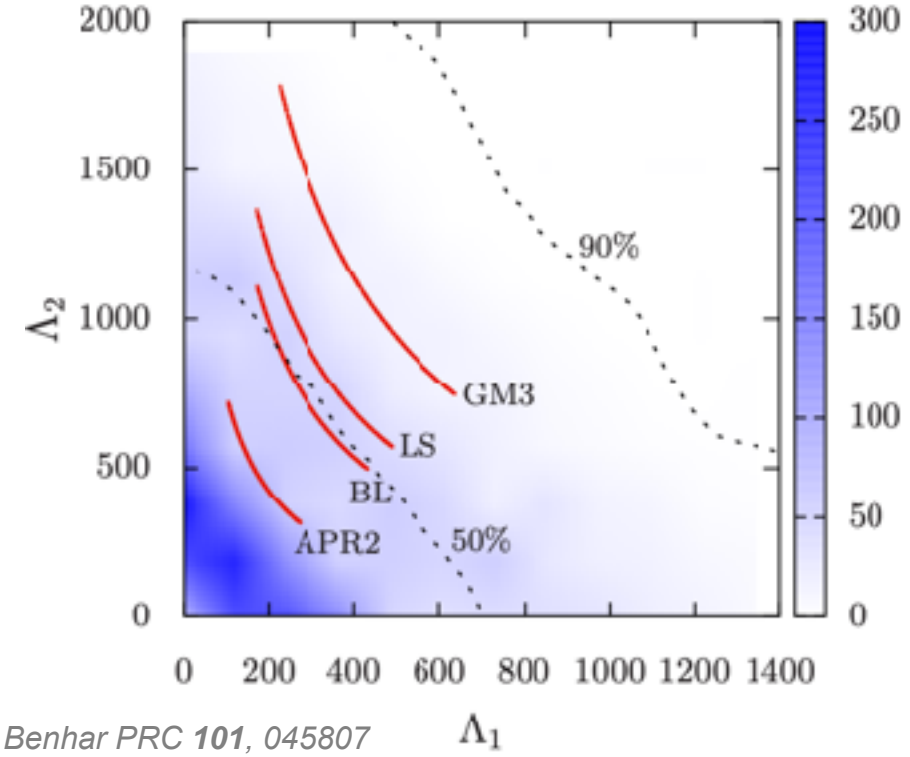

*A. Sabatucci, O. Benhar PRC **101**, 045807*

THE NUCLEAR MANY-BODY PROBLEM

In the low-energy regime, quark and gluons are confined within hadrons and the relevant degrees of freedoms are protons, neutrons, and pions

Effective field theories are the link between QCD and nuclear observables.

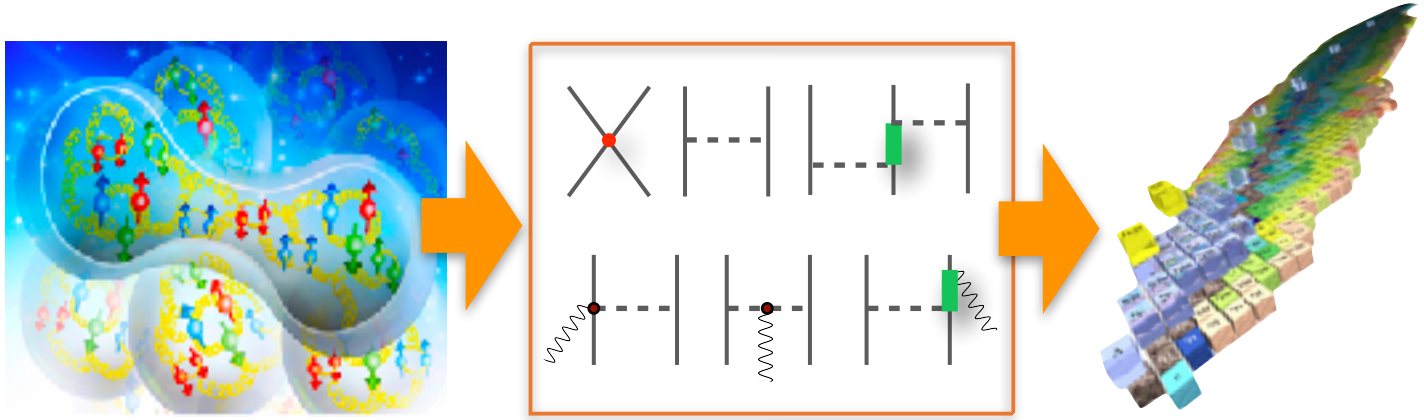

$$H = \sum_i \frac{\mathbf{p}_i^2}{2m} + \sum_{i<j} v_{ij} + \sum_{i<j<k} V_{ijk} \qquad J = \sum_i j_i + \sum_{i<j} j_{ij}$$

NUCLEAR MANY-BODY METHODS

Non relativistic many body theory aims at solving the many-body Schrödinger equation

$$H\Psi_0(x_1,\ldots,x_A) = E_0\Psi_0(x_1,\ldots,\ldots,x_A) \quad \longleftrightarrow \quad x_i \equiv \{\mathbf{r}_i, s_i^z, t_i^z\}$$

- Nuclear potentials are non-perturbative and spin-isospin dependent

$$H = \sum_i \frac{\mathbf{p}_i^2}{2m} + \sum_{i<j} v_{ij} + \sum_{i<j<k} V_{ijk}$$

$$\begin{cases} v_{ij} = \sum_{p=1}^{18} v^p(r_{ij}) O_{ij}^p \\ O_{ij}^{p=1,8} = (1, \sigma_{ij}, S_{ij}, \mathbf{L}\cdot\mathbf{S}) \times (1, \tau_{ij}) \end{cases}$$

- Nucleons are fermions, so the wave function must be anti-symmetric

$$\Psi_0(x_1,\ldots,x_i,\ldots,x_j,\ldots,x_A) = -\Psi_0(x_1,\ldots,x_j,\ldots,x_i,\ldots,x_A)$$

NUCLEAR MANY-BODY METHODS

- Hamiltonians and consistent currents are the main inputs to nuclear many-body methods
- These methods capitalize on high-performance computers to solve the Schrödinger equation with controlled approximation

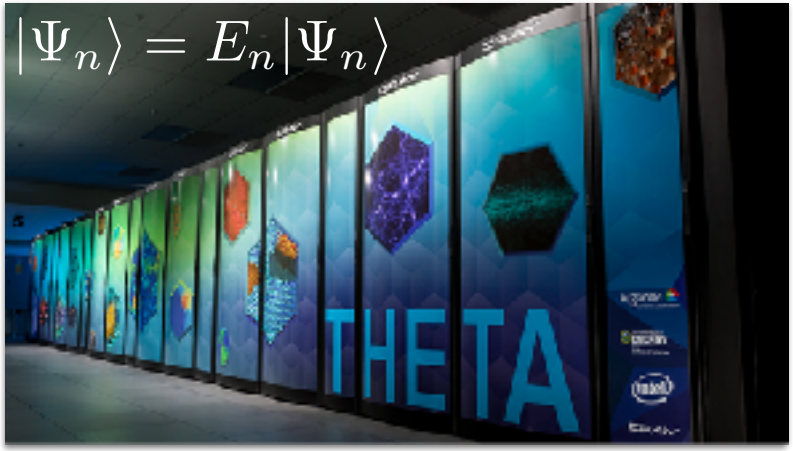

- Nuclear many-body calculations are continually battling against the “curse of dimensionality,” the rapid growth with complexity of computational resources needed.

COURSE OF DIMENSIONALITY

Configuration-Interaction

$$\Psi_0(x_1,\ldots,x_A) = \sum_n c_n \Phi_n(x_1,\ldots,x_A)$$

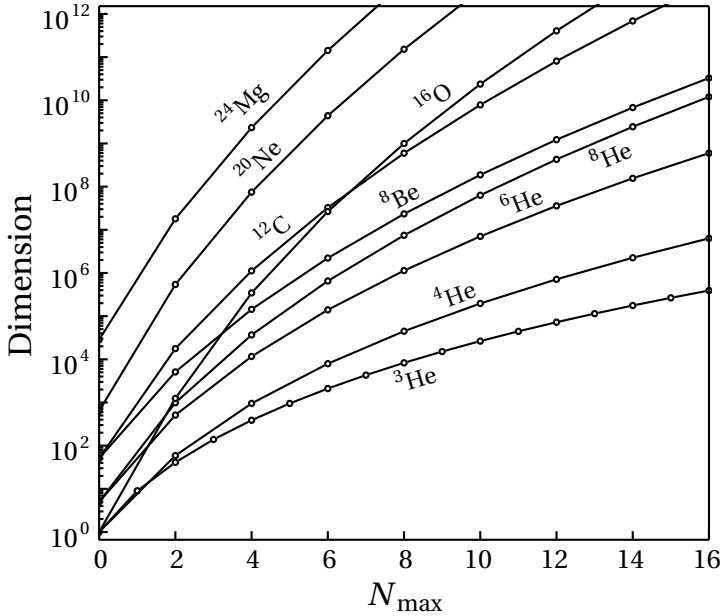

Green's function Monte Carlo

$$\lim_{\tau\to\infty} e^{-(H-E_0)\tau}\left|\Psi_T\right\rangle = c_0\left|\Psi_0\right\rangle$$

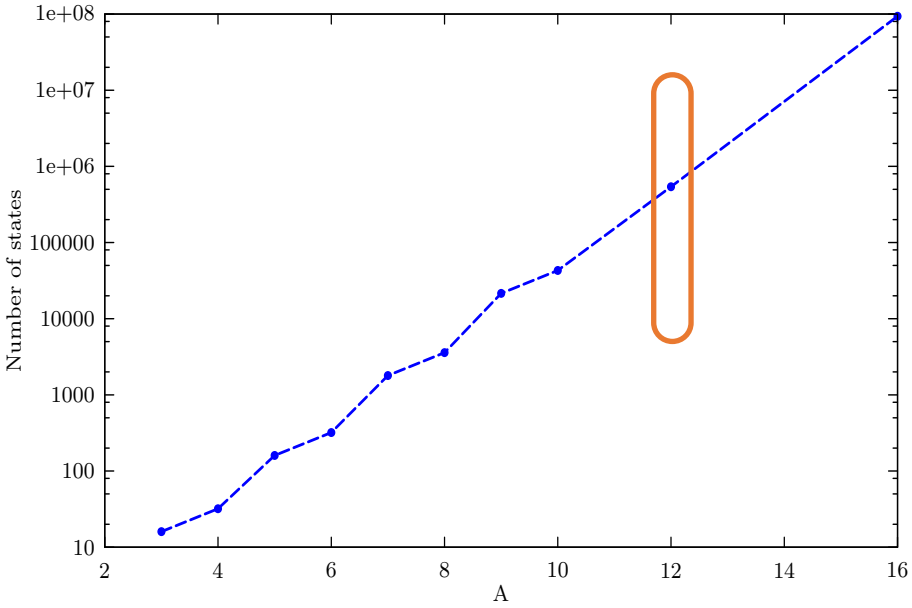

CONFIGURATION-INTERACTION METHODS

Full-CI (no-core shell model) is highly accurate, but limited to light nuclei

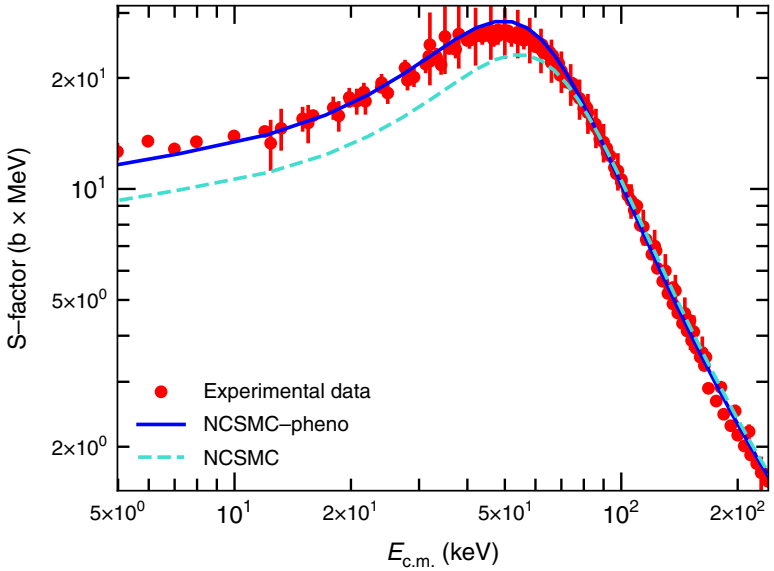

*G. Hupin et al., Nat. Comm. **10**, 351 (2019)*

Polynomially-scaling methods reach (much) larger systems with some approximations

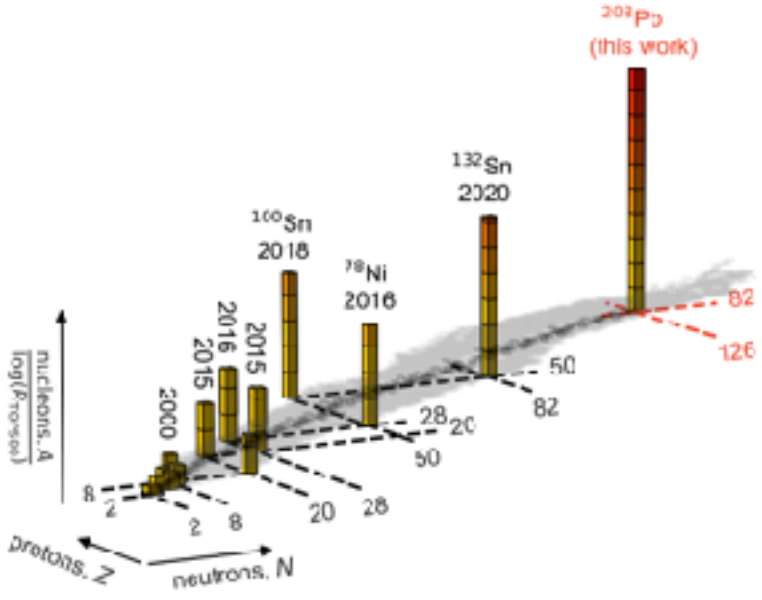

B. S. Hu et al., Nature Phys. (2022)

QUANTUM MONTE CARLO METHODS

Continuum nuclear quantum Monte Carlo make use of coordinate-space representation of many-body wave functions.

- They have no difficulties in treating “stiff” nuclear forces: test the convergence of nuclear EFTs;
- Access to high-momentum components of the nuclear wave functions;
- Limited to relatively light nuclear systems

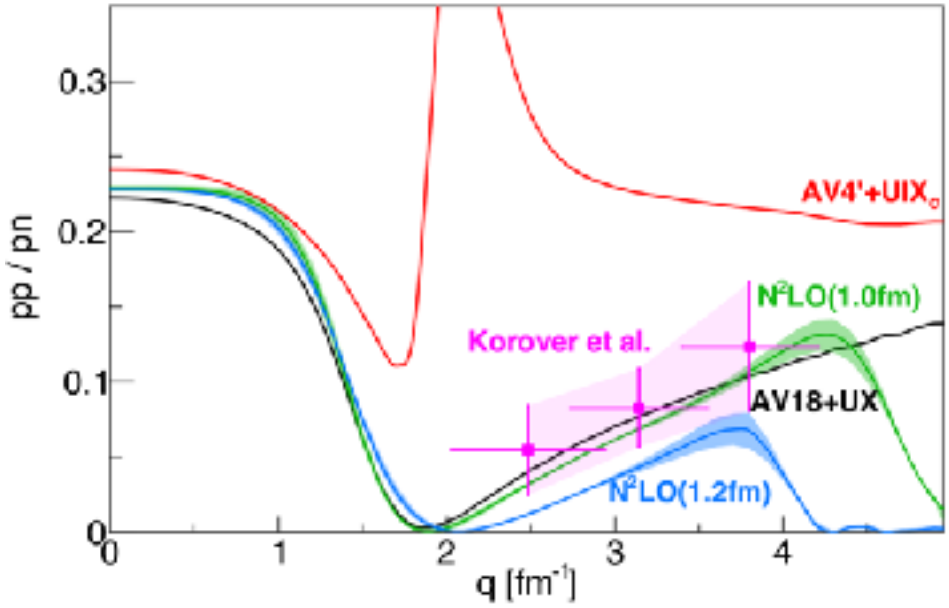

R. Cruz-Torres et al., Nature Phys. ***17*** *(2021) 3, 306*

NEURAL NETWORK QUANTUM STATES

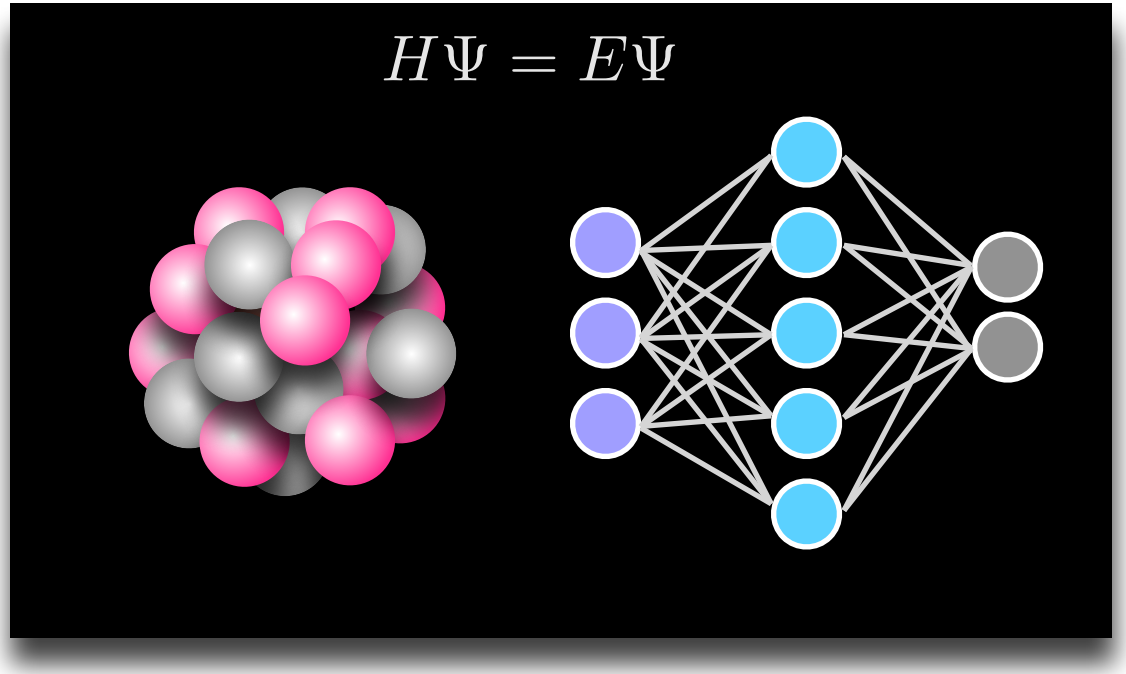

NEURAL-NETWORK QUANTUM STATES

Let's take a step back: spin problem  $H_{TIF} = -h\sum_i \sigma_i^x - \sum_{\langle i,j\rangle} \sigma_i^z \sigma_j^z$

Finding the exact solution of this equation is, in principle, an **exponentially hard problem**

$$|\Psi\rangle = c_{\uparrow\uparrow\uparrow\ldots}|\uparrow\uparrow\uparrow\ldots\rangle + c_{\downarrow\uparrow\uparrow\ldots}|\downarrow\uparrow\uparrow\ldots\rangle + \cdots + c_{\downarrow\downarrow\downarrow\ldots}|\downarrow\downarrow\downarrow\ldots\rangle$$

The majority of quantum states of physical interest have distinctive features and intrinsic structures

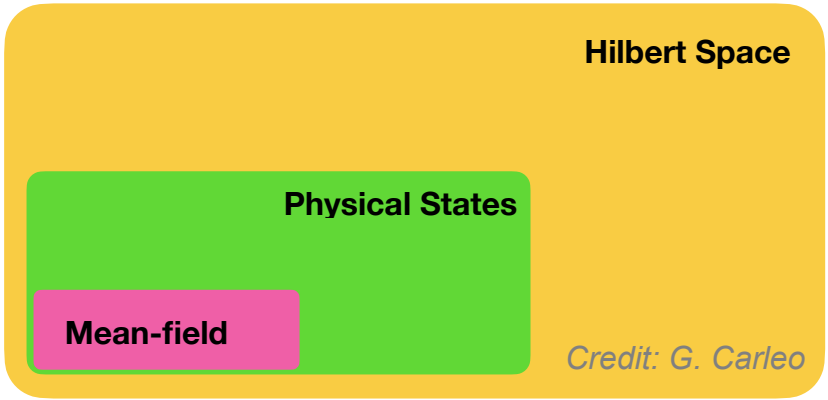

NEURAL-NETWORK QUANTUM STATES

$$\begin{cases} c_{\uparrow\uparrow\uparrow\ldots} \equiv \langle \uparrow\uparrow\uparrow \ldots | \Psi \rangle \equiv \Psi(\uparrow\uparrow\uparrow \ldots) \\ c_{\downarrow\uparrow\uparrow\ldots} \equiv \langle \downarrow\uparrow\uparrow \ldots | \Psi \rangle \equiv \Psi(\downarrow\uparrow\uparrow \ldots) \\ \\ c_{\downarrow\downarrow\downarrow\ldots} \equiv \langle \downarrow\downarrow\downarrow \ldots | \Psi \rangle \equiv \Psi(\downarrow\downarrow\downarrow \ldots) \end{cases} \quad \longleftrightarrow \quad c_S \equiv \langle S|\Psi\rangle \equiv \Psi(S)$$

Artificial neural networks (ANNs) can compactly represent complex high-dimensional functions;

$$\Psi(S) \simeq \langle S|\hat{\Psi}(\mathcal{W})\rangle \equiv \hat{\Psi}(S;\mathcal{W})$$

ANNs trained minimizing the energy, which is evaluated stochastically

$$E(\mathcal{W}) = \frac{\langle \hat{\Psi}(W)|H|\hat{\Psi}(W)\rangle}{\langle \hat{\Psi}(W)|\hat{\Psi}(W)\rangle} \simeq \sum_{S_n} \frac{\langle S_n|H|\hat{\Psi}(W)\rangle}{\langle S_n|\hat{\Psi}(W)\rangle} \qquad P(S_n) = |\langle S_n|\hat{\Psi}(W)\rangle|^2$$

NEURAL-NETWORK QUANTUM STATES

Giuseppe Carleo and Mathias Troyer demonstrated that RMBs outperform traditional Jastrows

$$\hat{\Psi}(S;\mathcal{W}) = \sum_{\{h_i\}} e^{\sum_j a_j \sigma_j^z + \sum_i b_i h_i + \sum_{ij} W_{ij} h_i \sigma_j^z}$$

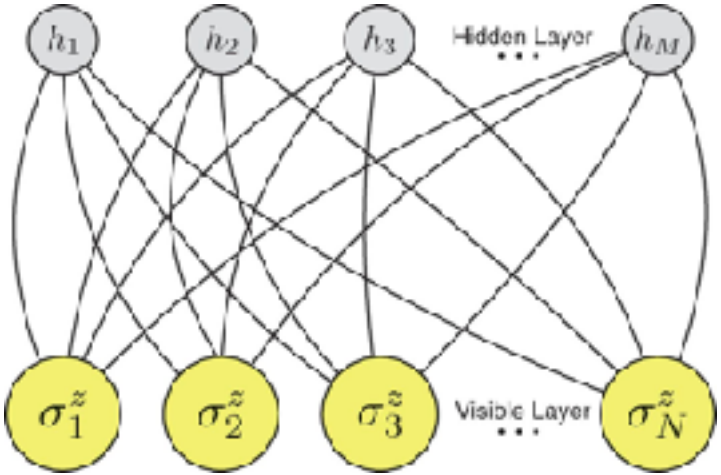

$$H_{TIF} = -h \sum_i \sigma_i^x - \sum_{\langle i,j \rangle} \sigma_i^z \sigma_j^z$$

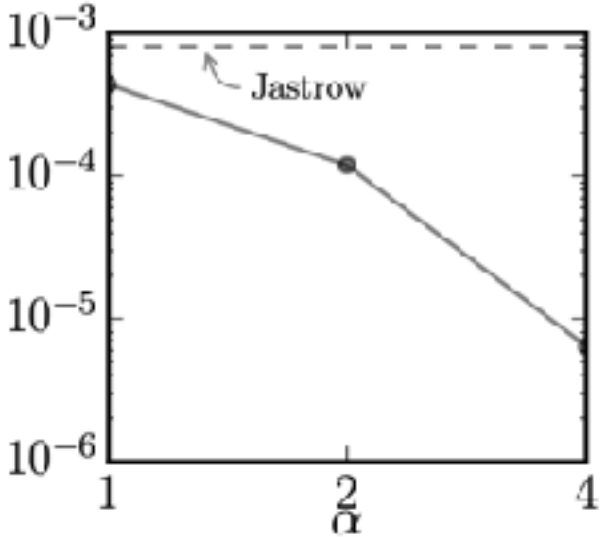

*G. Carleo et al. Science **355**, 602 (2017)*

PIONLESS EFT (INSPIRED) HAMILTONIAN

We take as input a LO pionless-EFT Hamiltonian that we contributed developing

$$H_{LO} = -\sum_i \frac{\vec{\nabla}_i^2}{2m_N} + \sum_{i<j} v_{ij} + \sum_{i<j<k} V_{ijk}$$

- NN potential: fit to np scattering lengths and effective radii and the deuteron binding energy

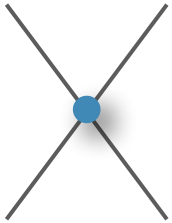

$$v_{ij}^{\rm CI} = \sum_{p=1}^{4} v^p(r_{ij}) O_{ij}^p \,,$$

$$O_{ij}^{p=1,4} = (1, \tau_{ij}, \sigma_{ij}, \sigma_{ij}\tau_{ij})$$

- 3NF adjusted to reproduce the ^{3}H binding energy.

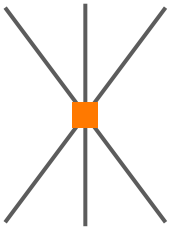

$$V_{ijk} = \tilde{c}_E \sum_{\rm cyc} e^{-(r_{ij}^2 + r_{jk}^2)/R_3^2}$$

*R. Schiavilla, AL, PRC **103**, 054003(2021)*

NEURAL SLATER-JASTROW ANSATZ

The ANN variational state is a product of mean-field state modulated by a flexible correlator factor

$$\Psi_{SJ}(X) = e^{J(X)}\Phi(X)$$

- The mean-field part is a Slater determinants of single-particle orbitals

$$\det \begin{bmatrix} \phi_1(\mathbf{x}_1) & \phi_1(\mathbf{x}_2) & \cdots & \phi_1(\mathbf{x}_N) \\ \phi_2(\mathbf{x}_1) & \phi_2(\mathbf{x}_2) & \cdots & \phi_2(\mathbf{x}_N) \\ \vdots & \vdots & \ddots & \vdots \\ \phi_N(\mathbf{x}_1) & \phi_N(\mathbf{x}_2) & \cdots & \phi_N(\mathbf{x}_N) \end{bmatrix}$$

- Each orbital is a FFNN that takes as input

$$\bar{\mathbf{r}}_i = \mathbf{r}_i - \mathbf{R}_{CM}$$

- The Jastrow is a permutation-invariant function of the single-particle coordinates

$$J(X) = \rho_F\left[\sum_i \vec{\phi}_{\mathcal{F}}(\bar{\mathbf{r}}_i, \mathbf{s}_i)\right]$$

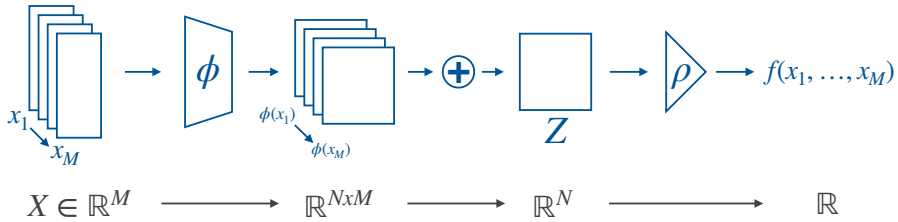

SAMPLING COORDINATES AND SPIN

The calculation of the observables involve integrating over 3A spatial and 2A spin-isospin variables

$$E_V = \frac{\langle \Psi_V | H | \Psi_V \rangle}{\langle \Psi_V | \Psi_V \rangle} = \frac{\sum_S \int dR |\Psi_V(R,S)|^2 \frac{\langle RS|H|\Psi_V\rangle}{\langle RS|\Psi_V\rangle}}{\sum_S \int dR |\Psi_V(R,S)|^2} .$$

We evaluate it stochastically using the Metropolis-Hastings Markov Chain Mote Carlo algorithm

Spatial move → $P_R = \frac{|\Psi_V(R',S)|^2}{|\Psi_V(R,S)|^2}$ Spin-isospin move → $P_S = \frac{|\Psi_V(R,S')|^2}{|\Psi_V(R,S)|^2}$

The observables are estimated by taking averages over the sampled configurations

$$\frac{\langle \Psi_V | O | \Psi_V \rangle}{\langle \Psi_V | \Psi_V \rangle} = \frac{1}{N_{\rm conf}} \sum_{\{R,S\}} O_L(R,S) \quad \Longleftrightarrow \quad P_V(R,S) = \frac{\Psi_V(R,S)|^2}{\sum_S \int dR |\Psi_V(R,S)|^2} .$$

STOCHASTIC RECONFIGURATION

The ANN is trained by performing an imaginary-time evolution in the variational manifold

$$(1 - H\delta\tau)|\Psi_V(\mathbf{p}_\tau)\rangle \simeq \Delta p^0 |\Psi_V(\mathbf{p}_\tau)\rangle + \sum_i \Delta p^i O^i |\Psi_V(\mathbf{p}_\tau)\rangle$$

During the optimization, then parameter are updated as

$$\mathbf{p}_{\tau+\delta\tau} = \mathbf{p}_\tau - \eta(S_\tau + \epsilon I)^{-1}\mathbf{g}_\tau$$

The gradient is supplemented by the quantum Fisher Information pre-conditioner

$$S_\tau^{ij} = \left\langle \frac{\partial \Psi_V(\mathbf{p}_\tau)}{\partial p_i} \middle| \frac{\partial \Psi_V(\mathbf{p}_\tau)}{\partial p_j} \right\rangle - \left\langle \frac{\partial \Psi_V(\mathbf{p}_\tau)}{\partial p_i} \right\rangle \left\langle \frac{\partial \Psi_V(\mathbf{p}_\tau)}{\partial p_j} \right\rangle$$

$$\gamma(\psi, \phi) = \arccos \sqrt{\frac{\langle\psi|\phi\rangle\langle\phi|\psi\rangle}{\langle\psi|\psi\rangle\langle\phi|\phi\rangle}}$$

*S. Sorella, Phys. Rev. B **64**, 024512 (2001)*

*J. Stokes, at al., Quantum **4**, 269 (2020).*

ADAPTIVE STOCHASTIC RECONFIGURATION

We use an adaptive learning rate with $10^{-7} < \eta < 10^{-2}$. It yields robust convergence patterns for all the nuclei and regulator choices that we have analyzed

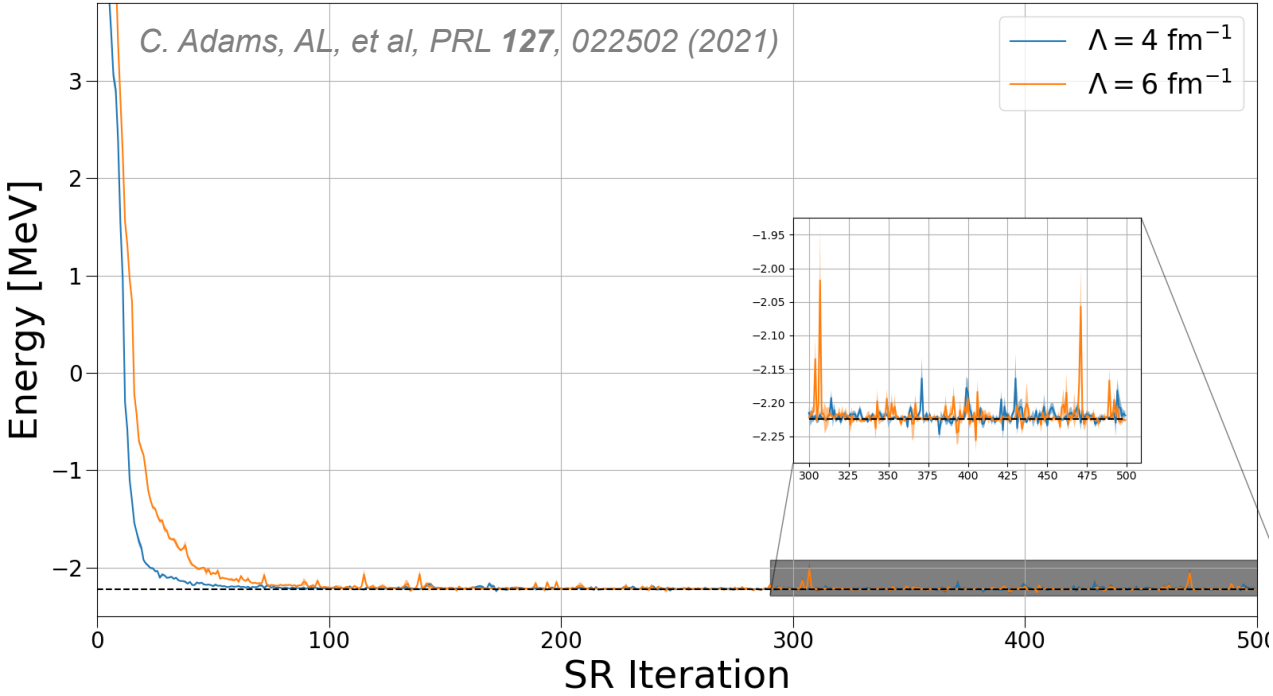

COMPARISON WITH QUANTUM MONTE CARLO

To further elucidate the quality of the ANN wave function we consider the point-nucleon density

$$\rho_N(r) = \frac{1}{4\pi r^2}\left\langle \Psi_V \middle| \sum_i \delta(r - |\mathbf{r}_i^{\text{int}}|) \middle| \Psi_V \right\rangle ,$$

^{3}H

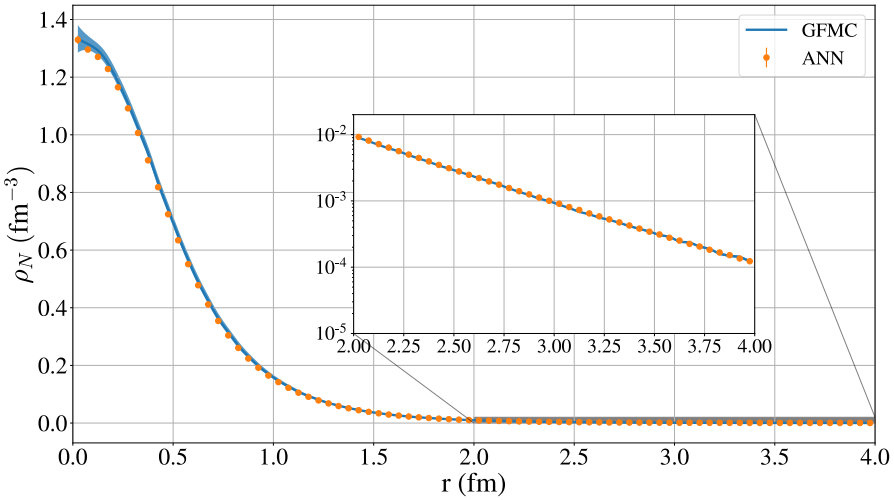

^{4}He

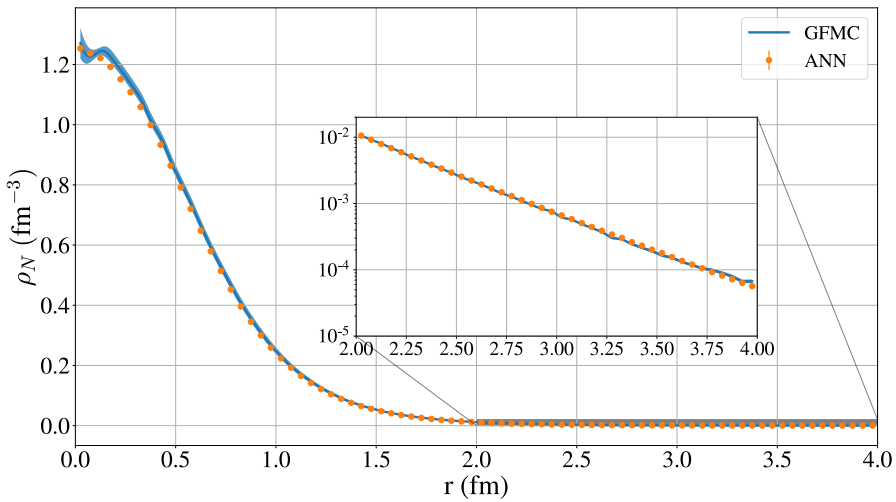

*C. Adams, AL, et al, PRL **127**, 022502 (2021)*

COMPARISON WITH QUANTUM MONTE CARLO

- The ANN Slater Jastrow ansatz outperforms conventional Jastrow correlations

	Λ	VMC-ANN	VMC-JS	GFMC	GFMC$_c$
^{2}H	4 fm^{-1}	$-2.224(1)$	$-2.223(1)$	$-2.224(1)$	-
	6 fm^{-1}	$-2.224(4)$	$-2.220(1)$	$-2.225(1)$	-
^{3}H	4 fm^{-1}	$-8.26(1)$	$-7.80(1)$	$-8.38(2)$	$-7.82(1)$
	6 fm^{-1}	$-8.27(1)$	$-7.74(1)$	$-8.38(2)$	$-7.81(1)$
^{4}He	4 fm^{-1}	$-23.30(2)$	$-22.54(1)$	$-23.62(3)$	$-22.77(2)$
	6 fm^{-1}	$-24.47(3)$	$-23.44(2)$	$-25.06(3)$	$-24.10(2)$

- Remaining differences with the GFMC are due to deficiencies in the Slater-Jastrow ansatz

$$\Psi_{SJ}(X) = e^{J(X)}\Phi(X)$$

C. Adams, AL, et al, PRL **127**, 022502 (2021)

HIDDEN NUCLEONS

The “hidden fermion” approach was recently introduced to model fermion wave functions

$$\langle RS|\Psi_{HF}\rangle = \begin{pmatrix} \phi_1(x_1) & \phi_1(x_2) & \phi_1(x_3) & \phi_1(x_4) & \phi_1(y_1) & \phi_1(y_2) & \phi_1(y_3) & \phi_1(y_4) \\ \phi_2(x_1) & \phi_2(x_2) & \phi_2(x_3) & \phi_2(x_4) & \phi_2(y_1) & \phi_2(y_2) & \phi_2(y_3) & \phi_2(y_4) \\ \phi_3(x_1) & \phi_3(x_2) & \phi_3(x_3) & \phi_3(x_4) & \phi_3(y_1) & \phi_3(y_2) & \phi_3(y_3) & \phi_3(y_4) \\ \phi_4(x_1) & \phi_4(x_2) & \phi_4(x_3) & \phi_4(x_4) & \phi_4(y_1) & \phi_4(y_2) & \phi_4(y_3) & \phi_4(y_4) \\ \chi_1(x_1) & \chi_1(x_2) & \chi_1(x_3) & \chi_1(x_4) & \chi_1(y_1) & \chi_1(y_2) & \chi_1(y_3) & \chi_1(y_4) \\ \chi_2(x_1) & \chi_2(x_2) & \chi_2(x_3) & \chi_2(x_4) & \chi_2(y_1) & \chi_2(y_2) & \chi_2(y_3) & \chi_2(y_4) \\ \chi_3(x_1) & \chi_3(x_2) & \chi_3(x_3) & \chi_3(x_4) & \chi_3(y_1) & \chi_3(y_2) & \chi_3(y_3) & \chi_3(y_4) \\ \chi_4(x_1) & \chi_4(x_2) & \chi_4(x_3) & \chi_4(x_4) & \chi_4(y_1) & \chi_4(y_2) & \chi_4(y_3) & \chi_4(y_4) \end{pmatrix}$$

Visible orbitals on visible coordinates

Visible orbitals on hidden coordinates

Hidden orbitals on visible coordinates

Hidden orbitals on hidden coordinates

*J. R. Moreno, et al., PNAS **119,** 2122059119(2022)*

HIDDEN NUCLEONS

The “hidden fermion” approach was recently introduced to model fermion wave functions

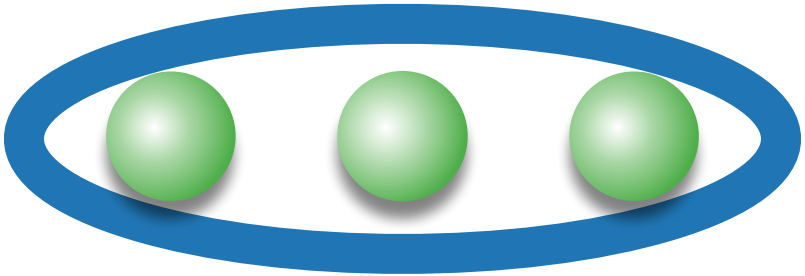

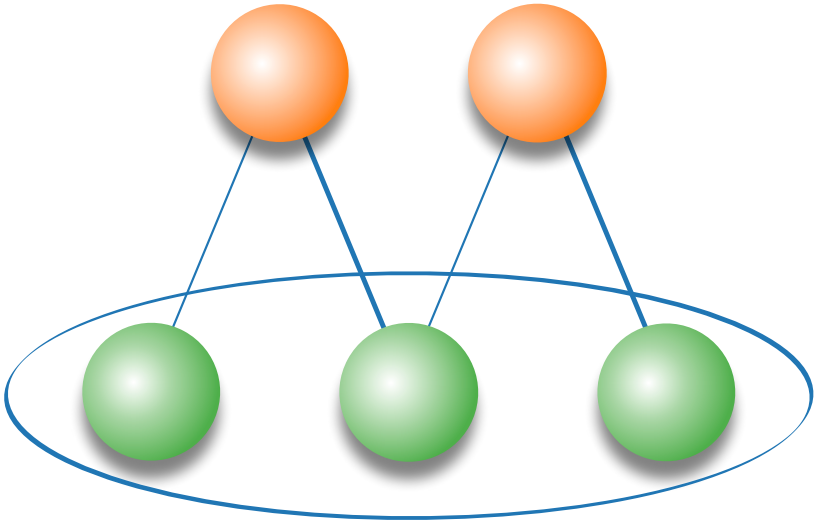

DISCRETE (POINT) SYMMETRIES

We enforce point-symmetries, such as parity and time reversal, into the hidden nucleon ansatz.

- We construct states with positive-definite parity by

$$\Psi^{P}_{HN}(R,S) \equiv \Psi_{HN}(R,S) + \Psi_{HN}(-R,S)\,.$$

- For even-even nuclei, such as ^{4}He and ^{16}O we can additionally enforce time-reversal symmetry

$$\Psi^{PT}_{HN}(R,S) \equiv \Psi^{P}_{HN}(R,S) + \Psi^{P}_{HN}(R,\theta S)\,,$$

where we define

$$\theta|S\rangle = -i\sigma^{y}_{1}|s^{1}_{z}\rangle \otimes -i\sigma^{y}_{2}|s^{2}_{z}\rangle \cdots \otimes -i\sigma^{y}_{A}|s^{A}_{z}\rangle$$

HIDDEN NUCLEONS FOR A=4 NUCLEI

We gauge the role of time reversal symmetry in ^{4}He by comparing again with the HH method

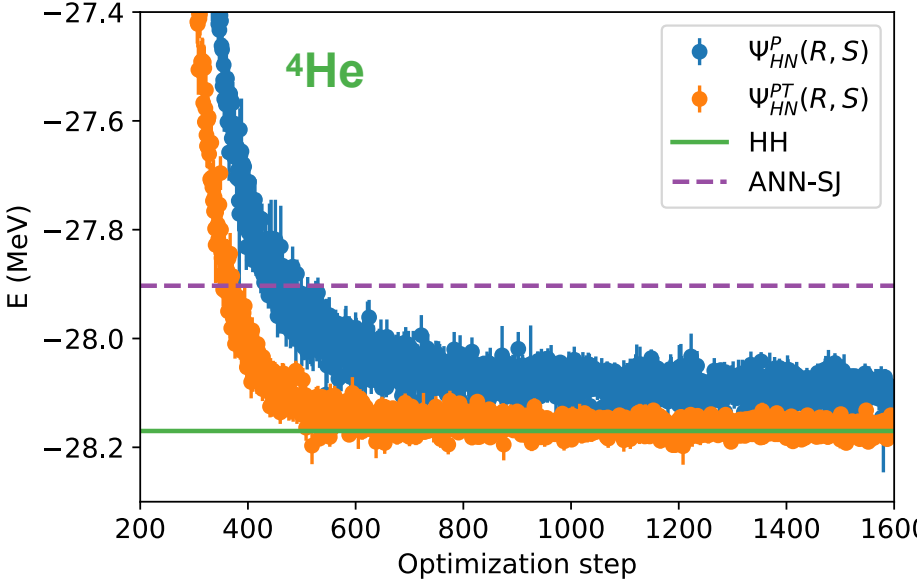

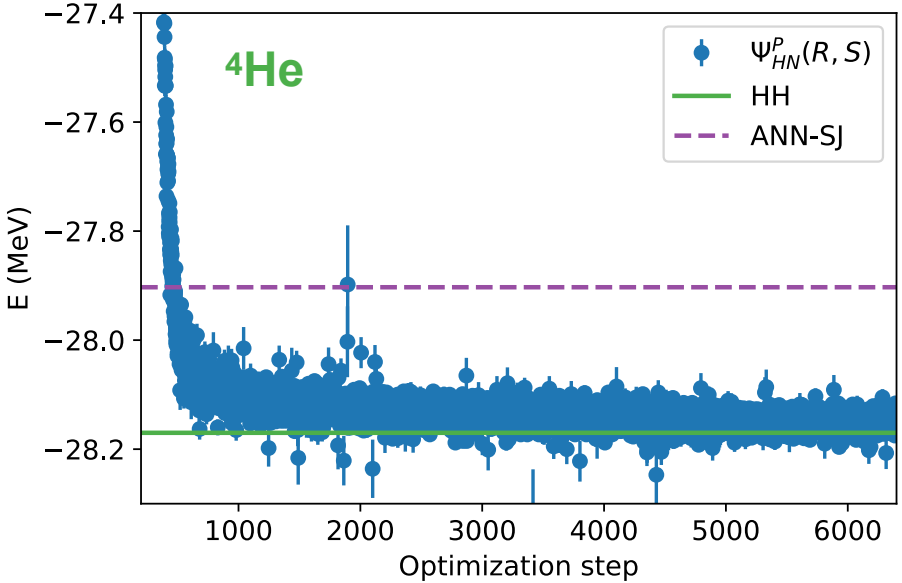

Imposing time reversal accelerates the training and augments the expressivity of the net for a fixed number of parameters

*AL, et al., Phys.Rev.Res. **4** (2022) 4, 043178*

NUCLEAR PHYSICS APPLICATIONS

We extend the reach of neural quantum states to ^{16}O

In addition to its ground-state energy, we evaluate the point-nucleon density of ^{16}O with A_h=16

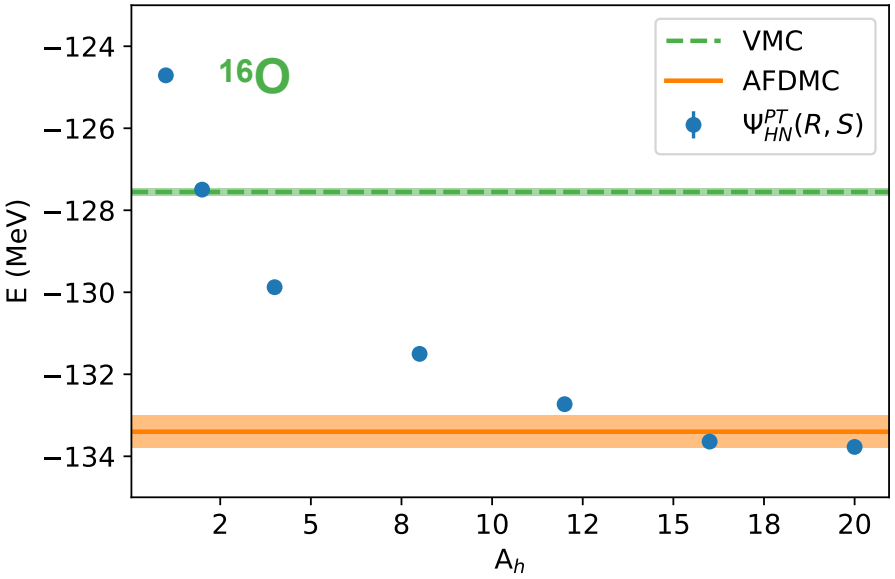

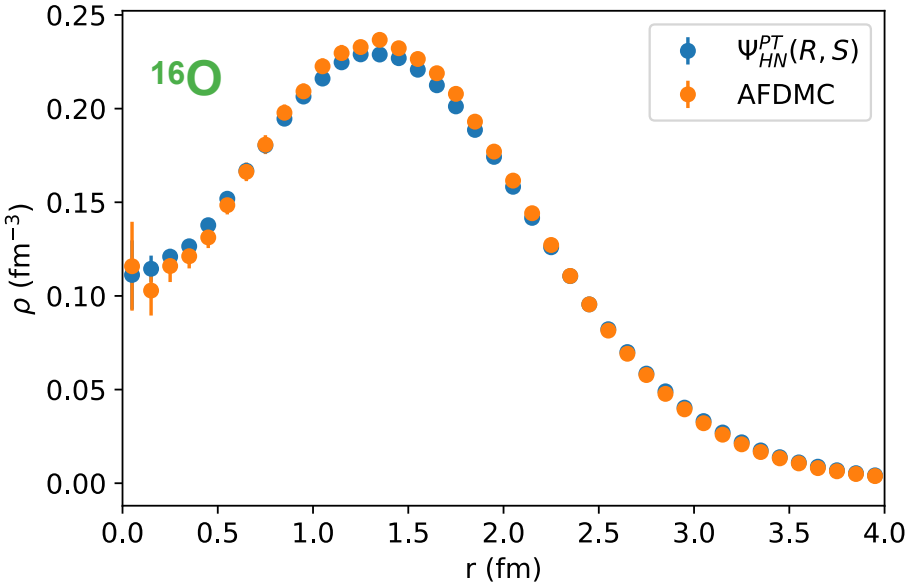

*AL, et al., Phys.Rev.Res. **4** (2022) 4, 043178*

INFINITE PERIODIC SYSTEMS

- We extended our approach to periodic systems, such us liquid ^{4}He and soft (gaussian) spheres

  ➡ Periodic ANN by construction: $\mathbf{r}_i \longrightarrow \tilde{\mathbf{r}}_i = \left\{ \sin\left(\frac{2\pi}{L}\mathbf{r}_i\right), \cos\left(\frac{2\pi}{L}\mathbf{r}_i\right) \right\}$

  ➡ Permutation invariant Deep-Sets ANN for computing bosons: $\Psi_V(R) = e^{\mathcal{U}(R)}$

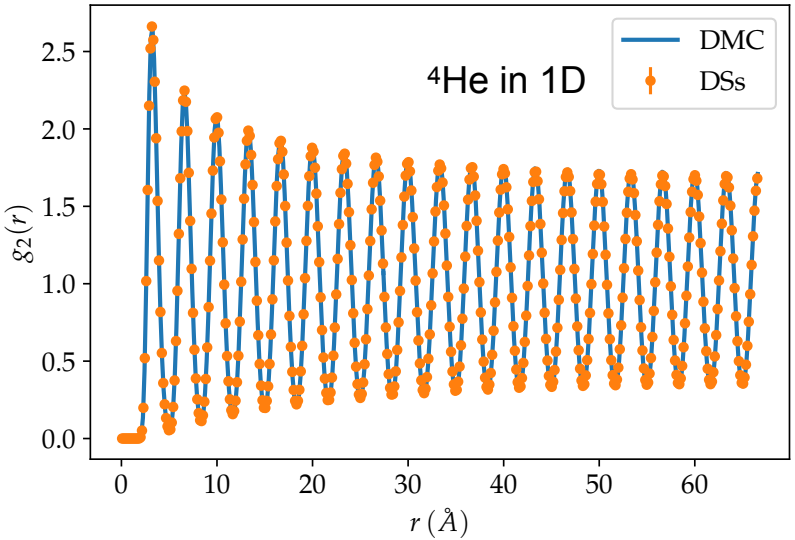

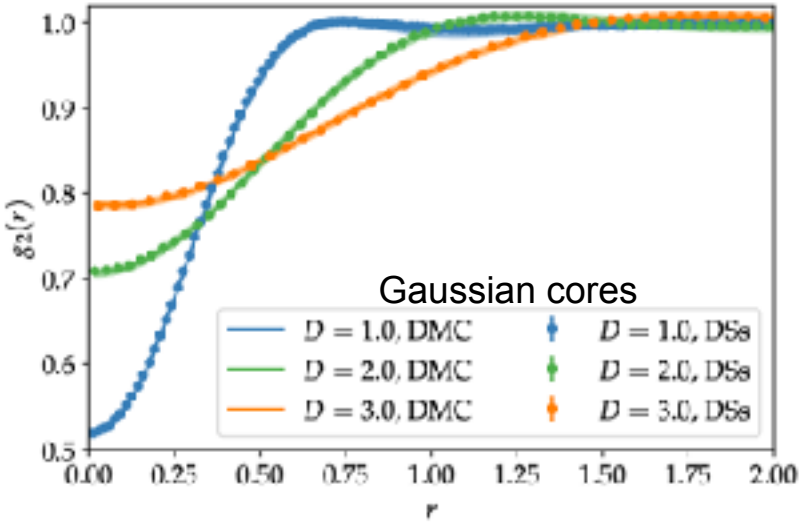

*G. Pescia, AL, et al., Phys. Rev .Res. **4** (2022) 023138*

DILUTE NEUTRON MATTER

We have introduced a periodic hidden-nucleons ansatz to model low-density neutron matter

The NQS ansatz converges to the unconstrained AFDMC energy, using a fraction of the computing time

- NQS: 100 hours on NVIDIA-A100
- AFDMC: 1.2 million hours on Intel-KNL

The hidden-nucleon ansatz captures the overwhelming majority of the correlation energy

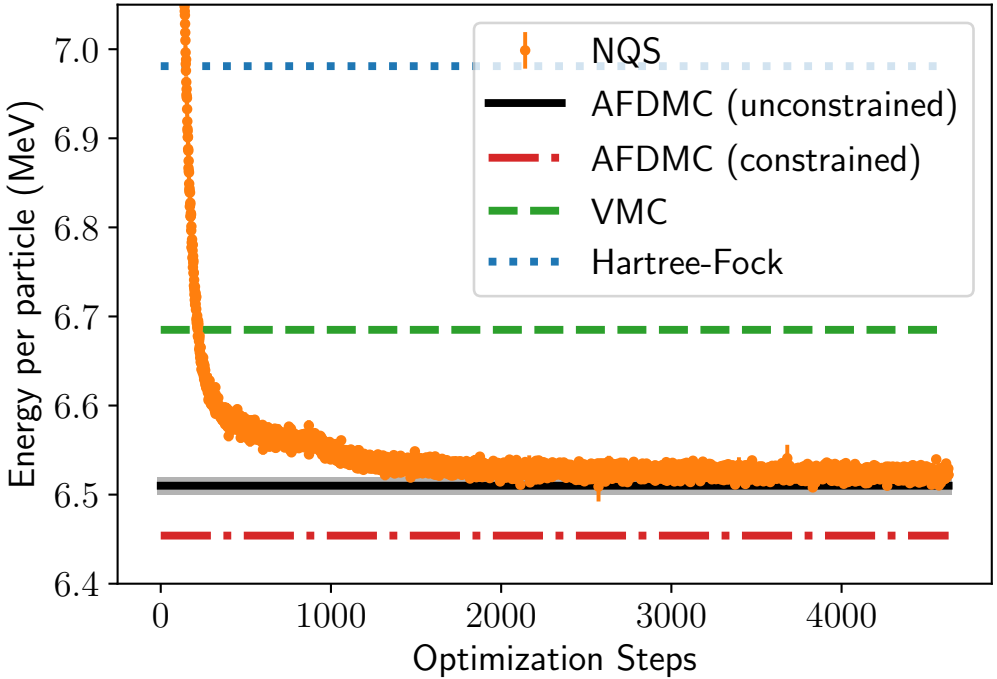

B. Fore, J. Kim, AL, arXiv:2212.04436 [nucl-th]

DILUTE NEUTRON MATTER

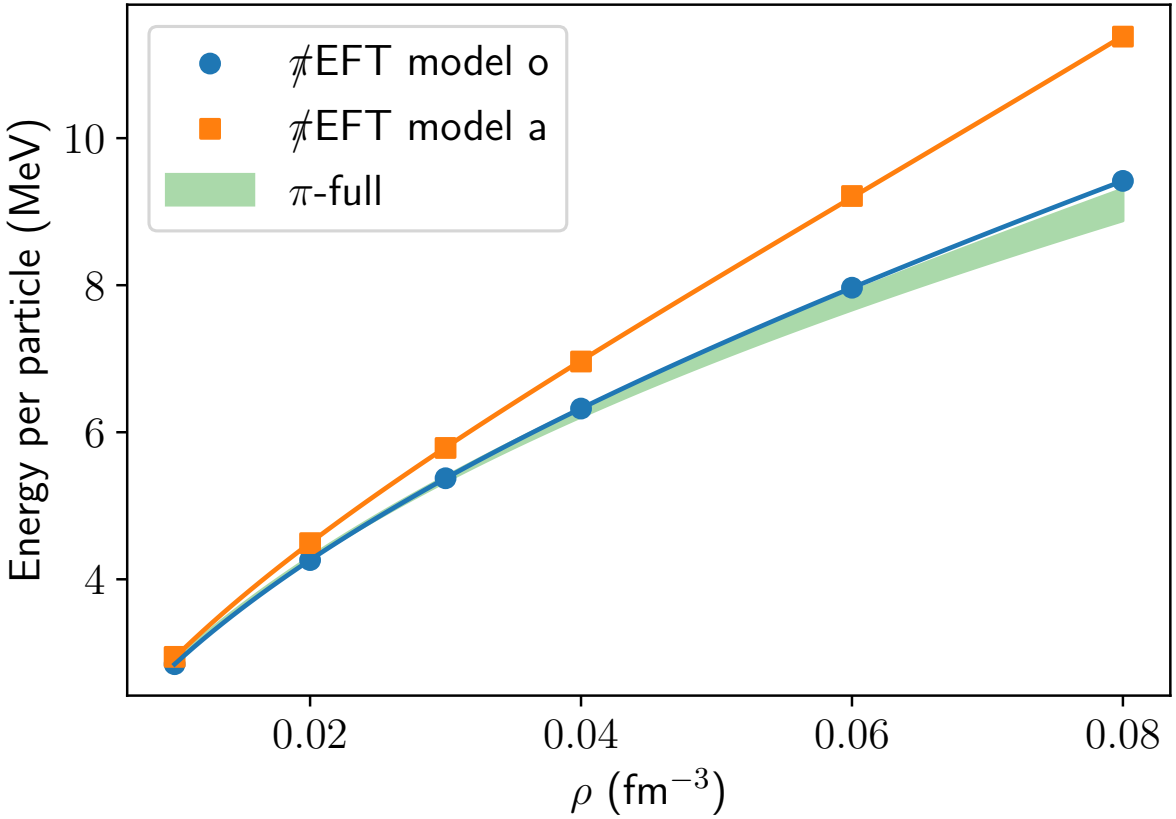

B. Fore, J. Kim, AL, arXiv:2212.04436 [nucl-th]

DILUTE NEUTRON MATTER

Low-density neutron matter is characterized by fascinating emergent quantum phenomena, such as the formation of Cooper pairs and the onset of superfluidity.

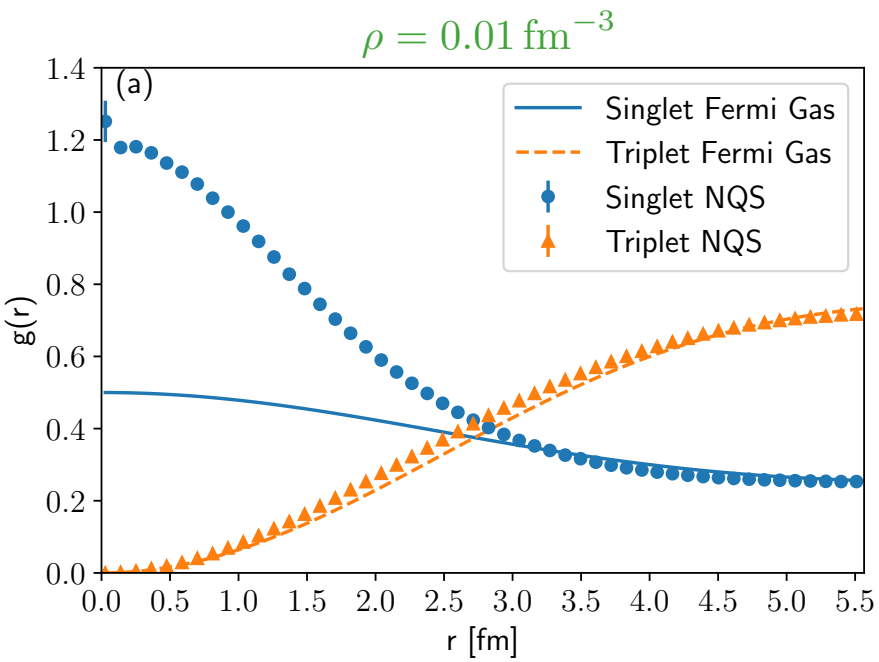

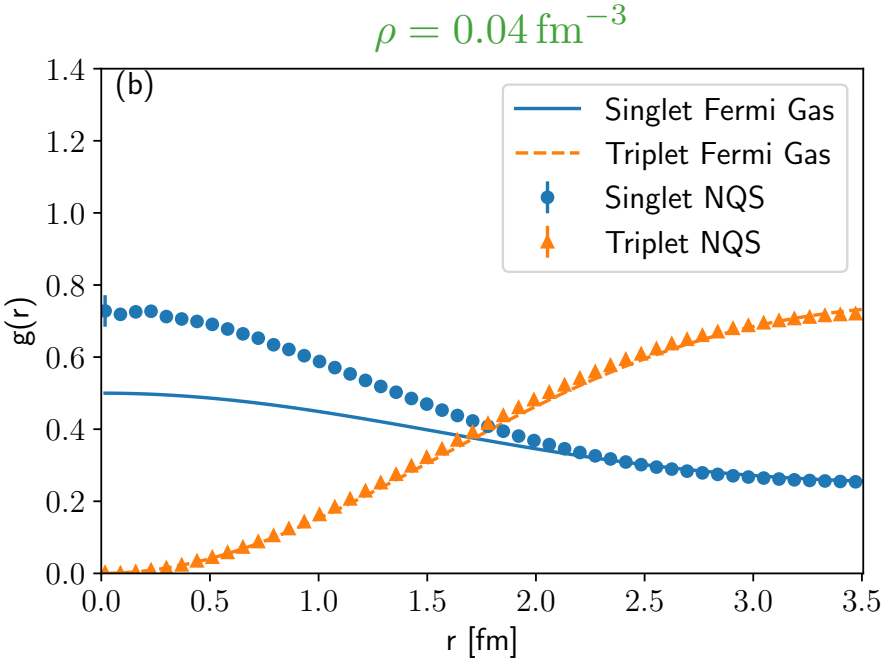

B. Fore, J. Kim, AL, arXiv:2212.04436 [nucl-th]

PART 1 AND 1/2

HOMOGENOUS ELECTRON GAS

We develop translation invariant NQS to study the Homogeneous Electron Gas.

$$H = -\frac{1}{2r_s^2}\sum_i^N \nabla^2_{\vec{r}_i} + \frac{1}{r_s}\sum_{i<j}^N \frac{1}{||\vec{r}_i - \vec{r}_j||} + \text{const.}$$

Start from a relatively simple Slater Jastrow ansatz

$$\Psi(X) = e^{J(X)}\Phi(X), \quad ; \quad \Phi(X) = \det \begin{bmatrix} \phi_1(\mathbf{x}_1) & \phi_1(\mathbf{x}_2) & \cdots & \phi_1(\mathbf{x}_N) \\ \phi_2(\mathbf{x}_1) & \phi_2(\mathbf{x}_2) & \cdots & \phi_2(\mathbf{x}_N) \\ \vdots & \vdots & \ddots & \vdots \\ \phi_N(\mathbf{x}_1) & \phi_N(\mathbf{x}_2) & \cdots & \phi_N(\mathbf{x}_N) \end{bmatrix}$$

Translation invariance: single-particle orbitals are plane-waves

$$\phi_i^{PW}(\mathbf{x}_j) = \mathrm{e}^{i\mathbf{k_i}\cdot\mathbf{r}_j}\langle\sigma_i|s_j\rangle\,,$$

HOMOGENOUS ELECTRON GAS

The nodal structure is improved with neural back-flow transformations $\mathbf{x}_i \longrightarrow \phi(\mathbf{x}_i; \mathbf{x}_{j\neq i})$

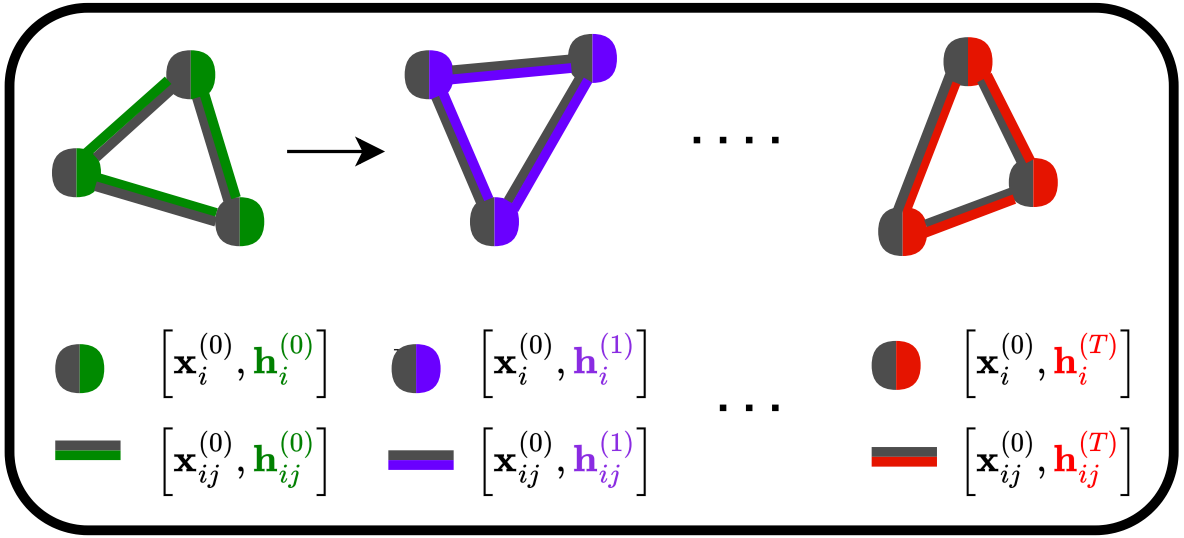

Translation-invariant (and periodic) by construction: $\longrightarrow$ $\mathbf{x}_i^{(0)} = \mathbf{e}, \qquad \mathbf{x}_{ij}^{(0)} = [\mathbf{r}_{ij}, ||\mathbf{r}_{ij}||, s_i \cdot s_j].$

G. Pescia, et al., 2305.08831 [cond-mat.quant-gas]

HOMOGENOUS ELECTRON GAS

Energies

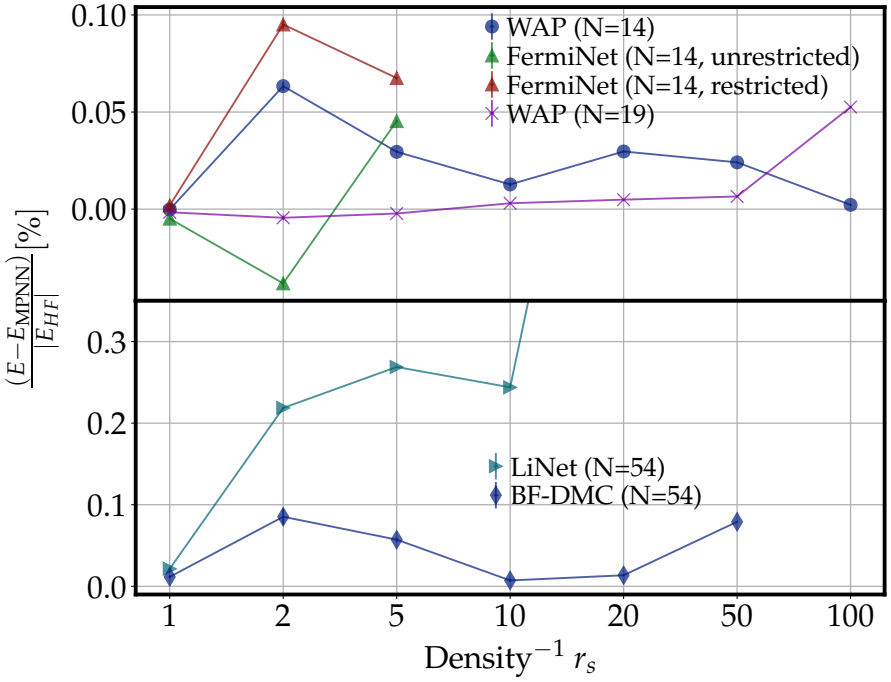

Correlation functions

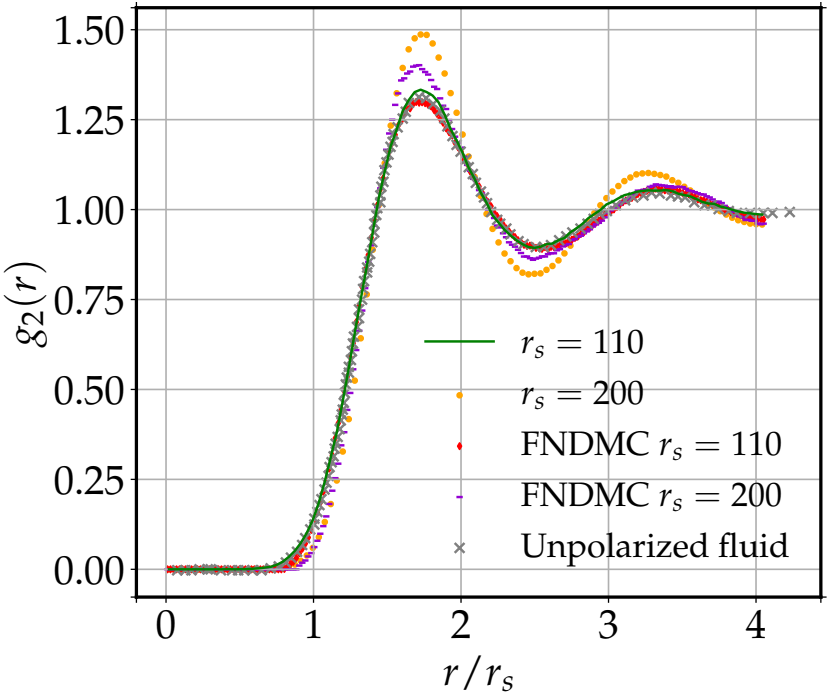

G. Pescia, et al., 2305.08831 [cond-mat.quant-gas]

COLD FERMI GASES

We developed periodic-NQS to solve the two-components Fermi gas in the BCS- BEC crossover region

- We model the 3D unpolarized gas of fermions with the Hamiltonian

$$H = -\frac{\hbar^2}{2m}\sum_i \nabla_i^2 + \sum_{ij} v_{ij}$$

- We use the Pöschl-Teller potential

$$v_{ij} = (s_i \cdot s_j - 1)V_0 \frac{\hbar^2}{2m}\frac{\mu^2}{\cosh^2(\mu r_{ij})}$$

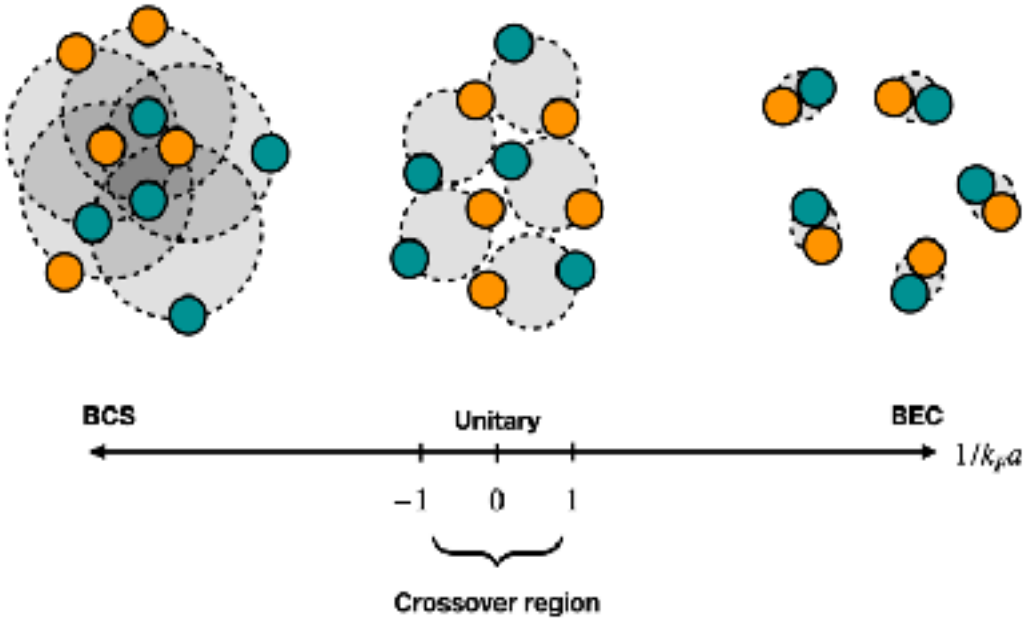

COLD FERMI GASES

Inspired by quantum Monte Carlo studies of dilute neutron matter, we developed a Pfaffian-Jastrow ansatz

$$\Phi_{PJ}(X) = \mathrm{pf}\begin{bmatrix} 0 & \phi(\mathbf{x}_1,\mathbf{x}_2) & \cdots & \phi(\mathbf{x}_1,\mathbf{x}_N) \\ \phi(\mathbf{x}_2,\mathbf{x}_1) & 0 & \cdots & \phi(\mathbf{x}_2,\mathbf{x}_N) \\ \vdots & \vdots & \ddots & \vdots \\ \phi(\mathbf{x}_N,\mathbf{x}_1) & \phi(\mathbf{x}_N,\mathbf{x}_2) & \cdots & 0 \end{bmatrix}$$

In order for the above matrix to be skew-symmetric, the neural pairing orbitals are taken to be

$$\phi(\mathbf{x}_i,\mathbf{x}_j) = \eta(\mathbf{x}_i,\mathbf{x}_j) - \eta(\mathbf{x}_j,\mathbf{x}_i),$$

Example: $$\mathrm{pf}\begin{bmatrix} 0 & \phi_{12} & \phi_{13} & \phi_{14} \\ -\phi_{12} & 0 & \phi_{23} & \phi_{24} \\ -\phi_{13} & -\phi_{23} & 0 & \phi_{34} \\ -\phi_{14} & -\phi_{24} & -\phi_{34} & 0 \end{bmatrix} = \phi_{12}\phi_{34} - \phi_{13}\phi_{24} + \phi_{14}\phi_{23}$$

J. Kim, B. Fore, AL, et al. arXiv:2305.08831

COLD FERMI GASES

We benchmark the performances of the neural-network quantum states with DMC calculations

- Slater - Jastrow

$$e^{J(X)} \times \begin{bmatrix} \phi_1(\mathbf{x}_1) & \phi_1(\mathbf{x}_2) & \cdots & \phi_1(\mathbf{x}_N) \\ \phi_2(\mathbf{x}_1) & \phi_2(\mathbf{x}_2) & \cdots & \phi_2(\mathbf{x}_N) \\ \vdots & \vdots & \ddots & \vdots \\ \phi_N(\mathbf{x}_1) & \phi_N(\mathbf{x}_2) & \cdots & \phi_N(\mathbf{x}_N) \end{bmatrix}$$

- Pfaffian - Jastrow

$$e^{J(X)} \times \mathrm{pf} \begin{bmatrix} 0 & \phi(\mathbf{x}_1, \mathbf{x}_2) & \cdots & \phi(\mathbf{x}_1, \mathbf{x}_N) \\ \phi(\mathbf{x}_2, \mathbf{x}_1) & 0 & \cdots & \phi(\mathbf{x}_2, \mathbf{x}_N) \\ \vdots & \vdots & \ddots & \vdots \\ \phi(\mathbf{x}_N, \mathbf{x}_1) & \phi(\mathbf{x}_N, \mathbf{x}_2) & \cdots & 0 \end{bmatrix}$$

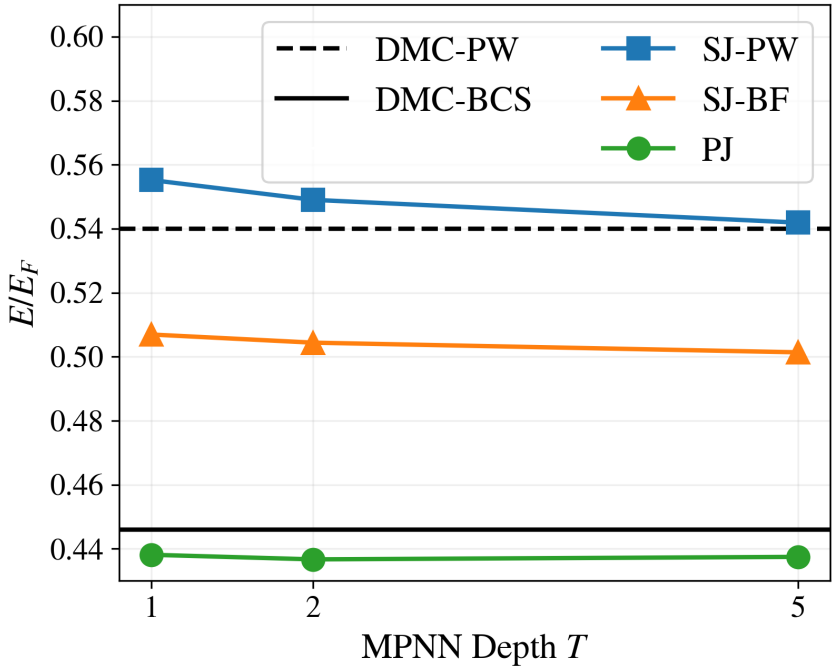

J. Kim, B. Fore, AL, et al. arXiv:2305.08831

COLD FERMI GASES

We proved that neural-network quantum state can model the BCS - BEC crossover better than DMC

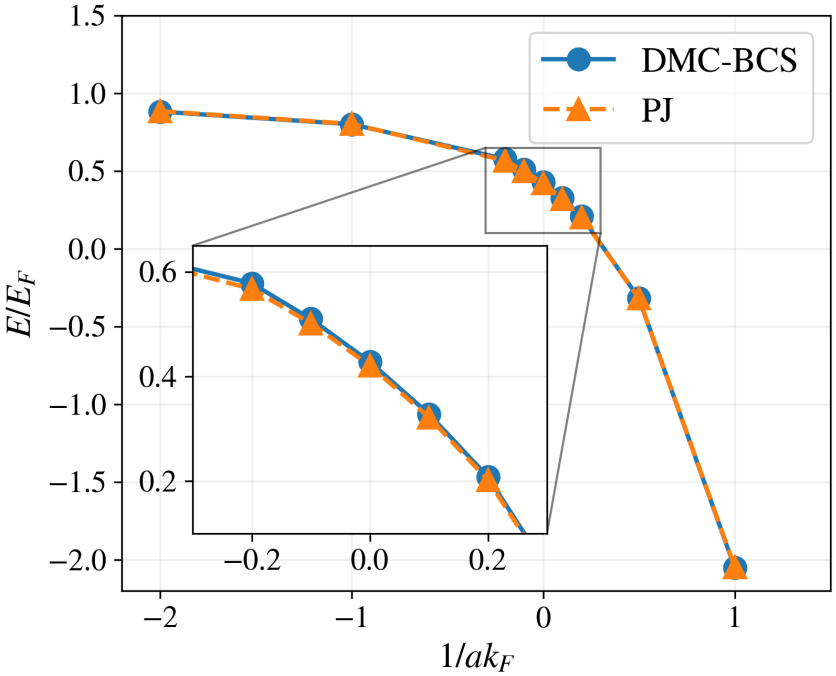

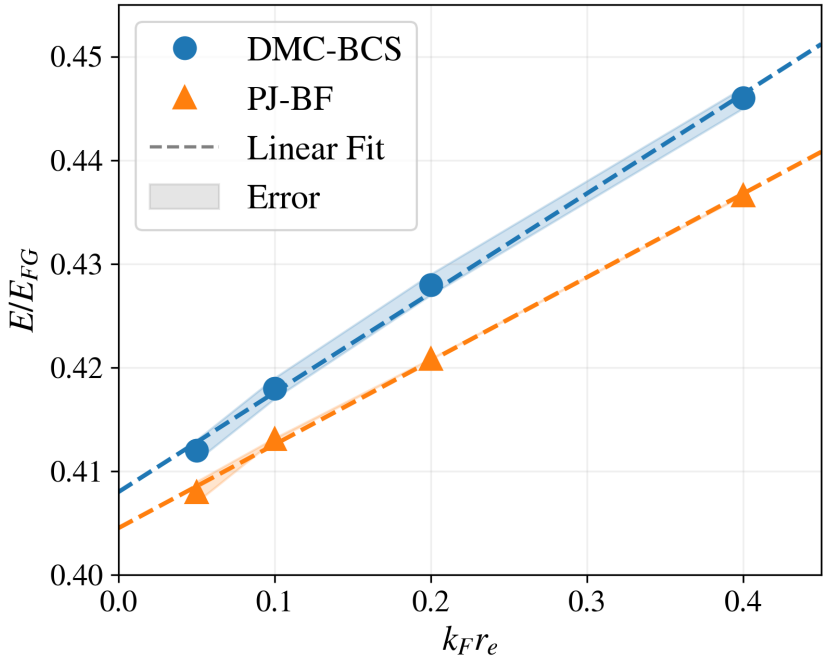

J. Kim, B. Fore, AL, et al. arXiv:2305.08831

COLD FERMI GASES

The spin-dependent two-body radial distribution functions capture the probability density of finding two particles with specific spin orientations at a given separation distance

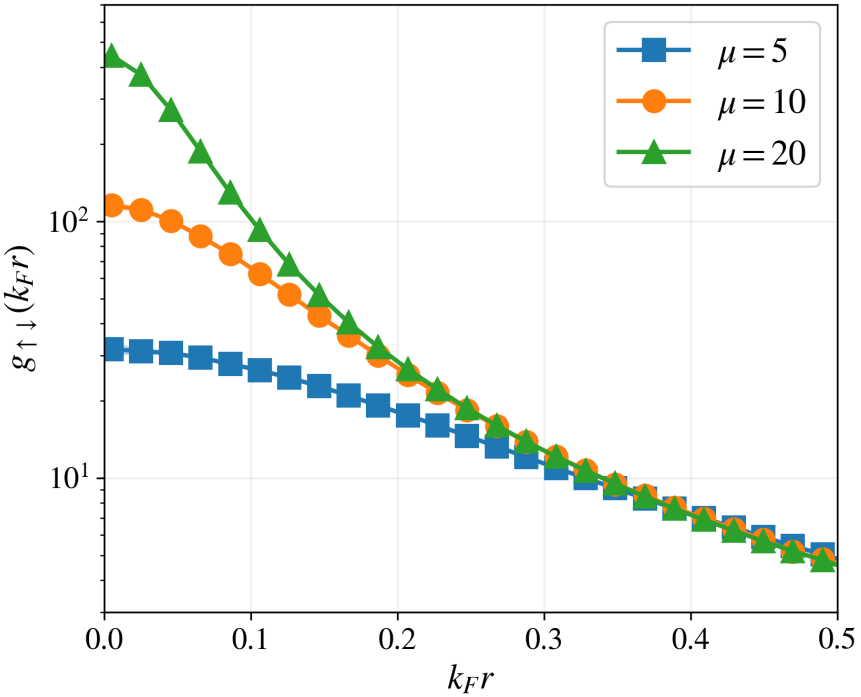

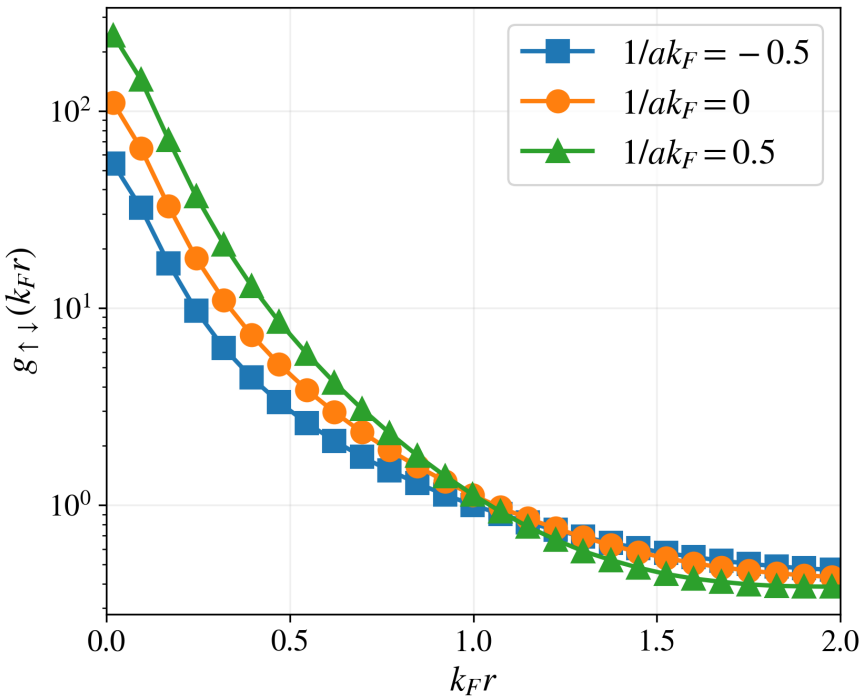

J. Kim, B. Fore, AL, et al. arXiv:2305.08831

COLD FERMI GASES

The pairing gap can be estimated from odd-even staggering

$$\Delta_N = \frac{(-1)^N}{2}[2E_N - E_{N+1} - E_{N-1}]$$

The unpaired particle has a defined momentum that fit the box

$$\mathrm{pf}\begin{bmatrix} 0 & \phi_{12} & \cdots & \phi_{1N} & \psi_k(1) \\ -\phi_{12} & 0 & \cdots & \phi_{2N} & \psi_k(2) \\ \vdots & \vdots & \ddots & \vdots & \vdots \\ -\phi_{1N} & -\phi_{2N} & \cdots & 0 & \psi_k(N) \end{bmatrix}$$

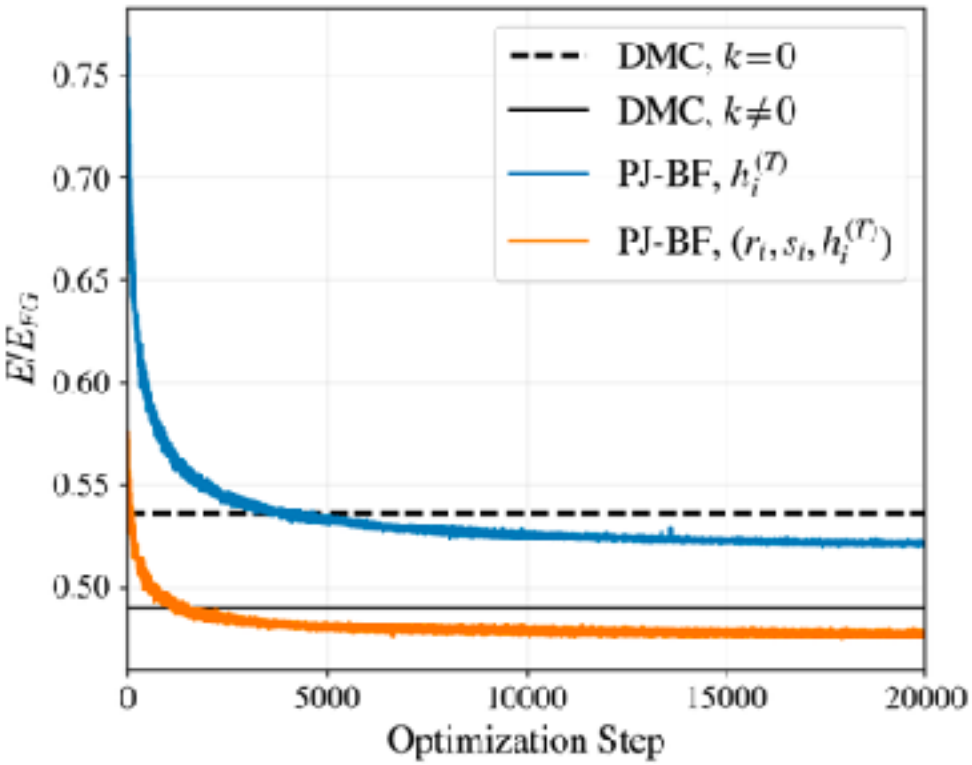

J. Kim, B. Fore, AL, et al. arXiv:2305.08831

BACK TO NUCLEI, WITH MPNN

Even with just one hidden-nucleon we do better than AFDMC for medium-mass nuclei

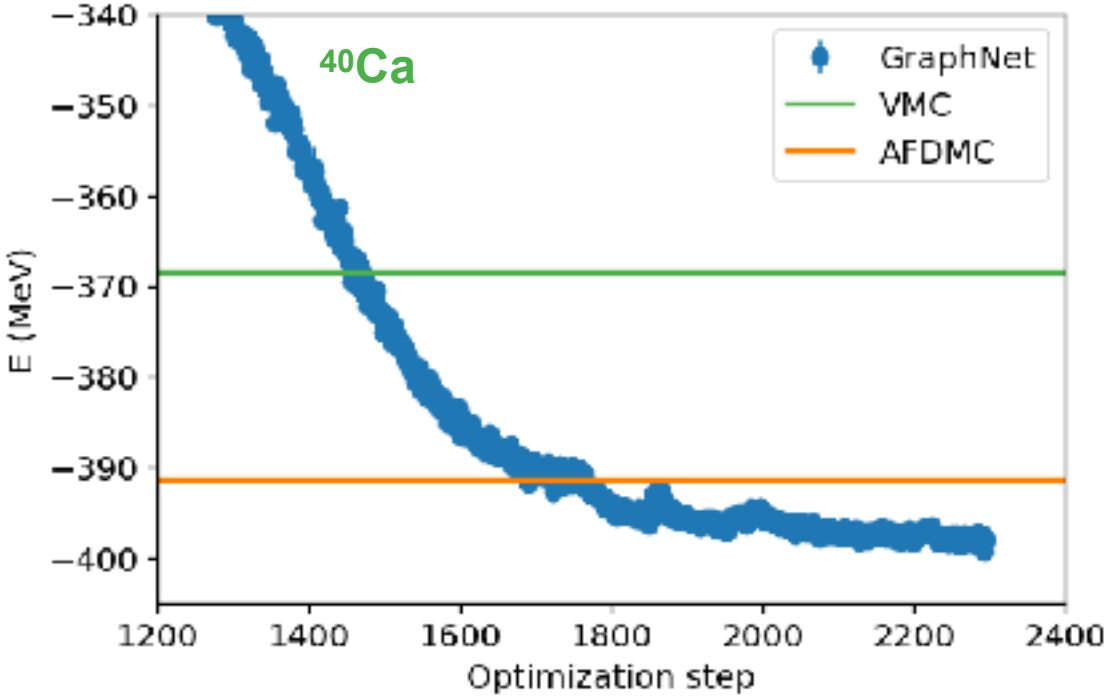

BACK TO NUCLEI, WITH MPNN

In addition to energies and single-particle densities, we can compute electroweak properties

^{6}Li

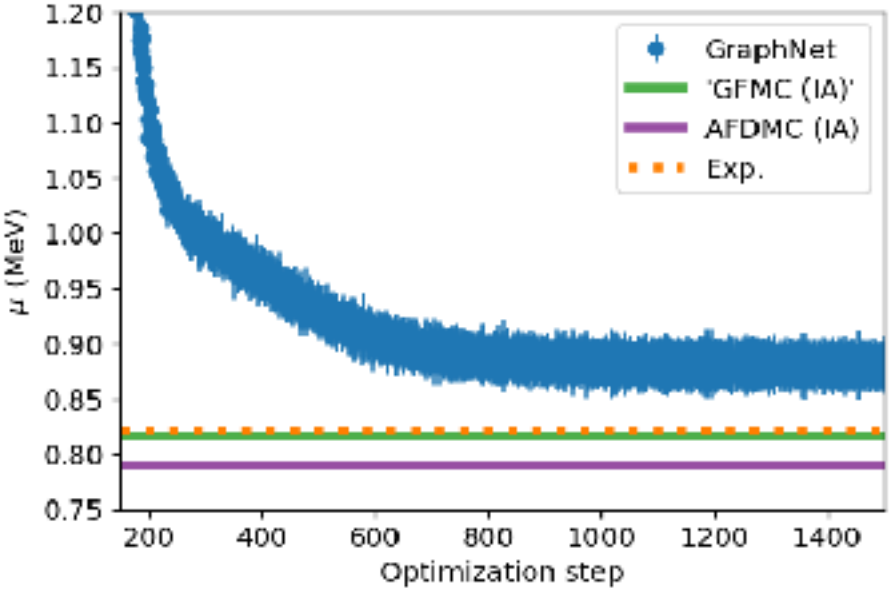

^{7}Li

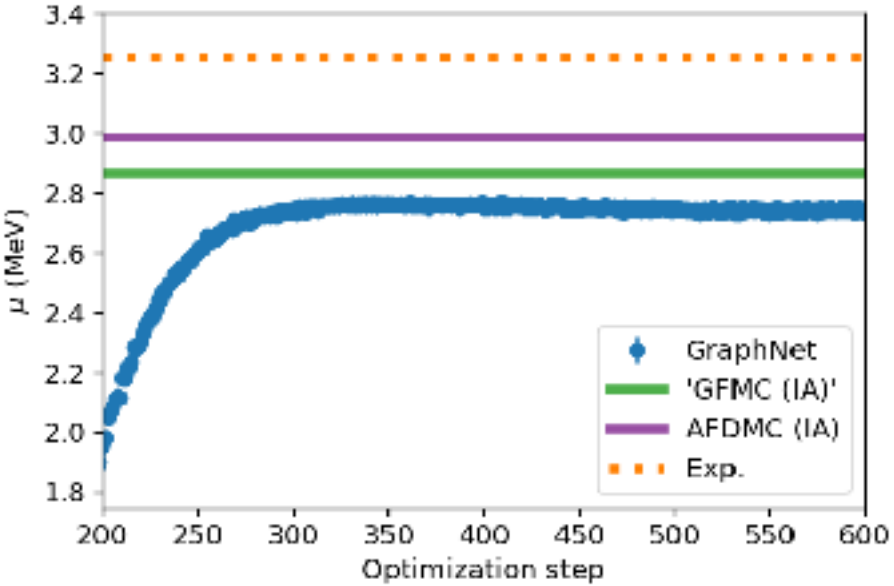

CONCLUSIONS

Neural network quantum states are extending the reach of conventional QMC methods

- Favorable scaling with the number of fermions;
- Universal and accurate approximations for fermion wave functions;
- Suitable for confined and periodic systems;
- Scalable to leadership-class hybrid CPU/GPU computers

PERSPECTIVES

- NQS calculations of medium-mass stable and exotic nuclei relevant to FRIB and ATLAS

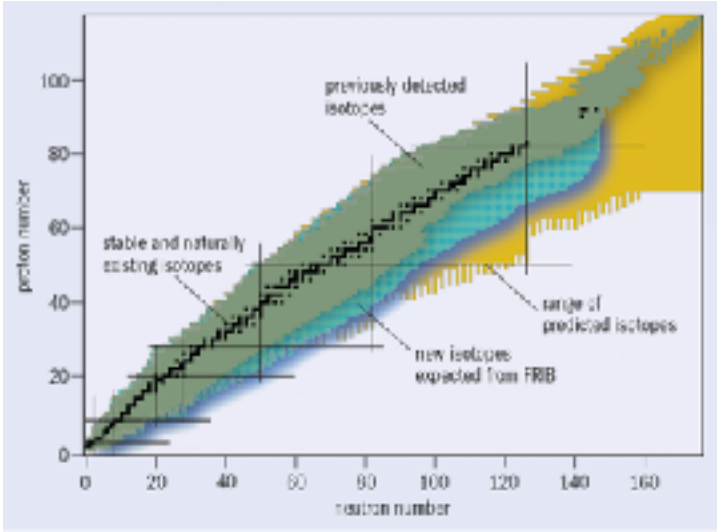

- High-precision electroweak transitions, including magnetic moments and beta-decay rates;
- Compute low-density isospin-asymmetric nucleonic matter: the flexibility of NQS will allow us to see self-emerging clustering in the low-density region;

PERSPECTIVES

- Access “real-time” dynamics: the prototypal exponentially-hard problem in many-body theory

$$\mathcal{D}\left(|\Psi(\mathbf{p}_{t+\delta t})\rangle, e^{-iHt}|\Psi(\mathbf{p}_t)\rangle\right)^2 = \arccos\left(\sqrt{\frac{\langle\Psi(\mathbf{p}_{t+\delta t})|e^{-iHt}|\Psi(\mathbf{p}_t)\rangle\langle\Psi(\mathbf{p}_t)|e^{iHt}|\Psi(\mathbf{p}_{t+\delta t})\rangle}{\langle\Psi(\mathbf{p}_{t+\delta t})|\Psi(\mathbf{p}_{t+\delta t})\rangle\langle\Psi(\mathbf{p}_t)|\Psi(\mathbf{p}_{\tau+\delta t})\rangle}}\right)^2$$

- Relevant for: fusion, lepton-nucleus scattering, and collective neutrino oscillation;

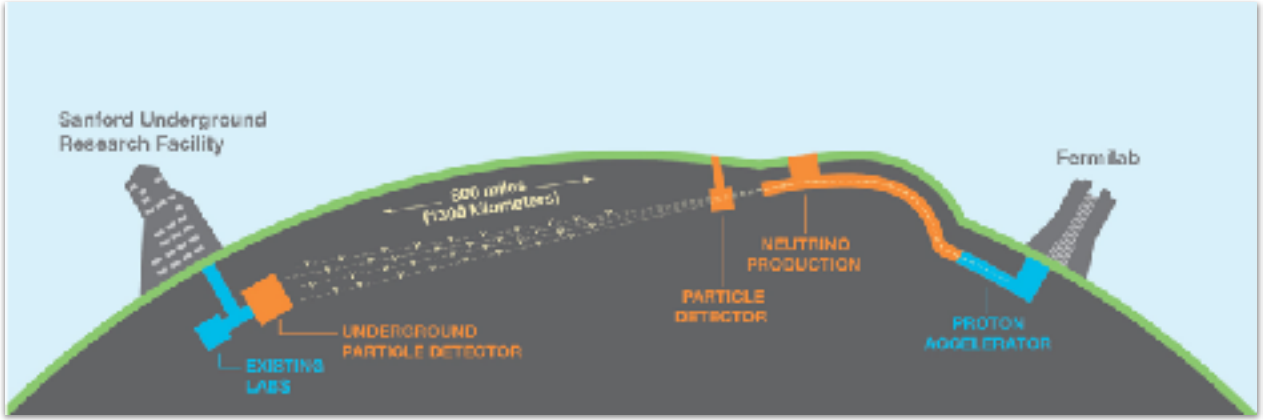

THANK YOU

MACHINE-LEARNING THE DEUTERON

ANNs were recently applied to solve the deuteron in momentum space using the N3LO Entem-Machleidt chiral-EFT nucleon-nucleon force

*Keeble, Rios, PLB **809**, 135743 (2020)*

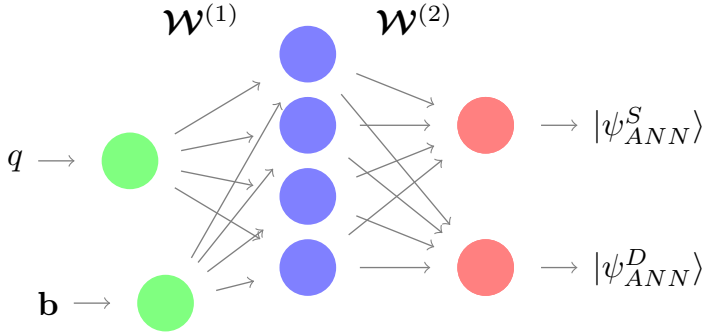

The parameters of the ANN are optimized minimizing the variational energy using RMSprop

$$E^{\mathcal{W}} = \frac{\left\langle \Psi^{\mathcal{W}}_{\mathrm{ANN}} \middle| \hat{H} \middle| \Psi^{\mathcal{W}}_{\mathrm{ANN}} \right\rangle}{\left\langle \Psi^{\mathcal{W}}_{\mathrm{ANN}} \middle| \Psi^{\mathcal{W}}_{\mathrm{ANN}} \right\rangle}$$

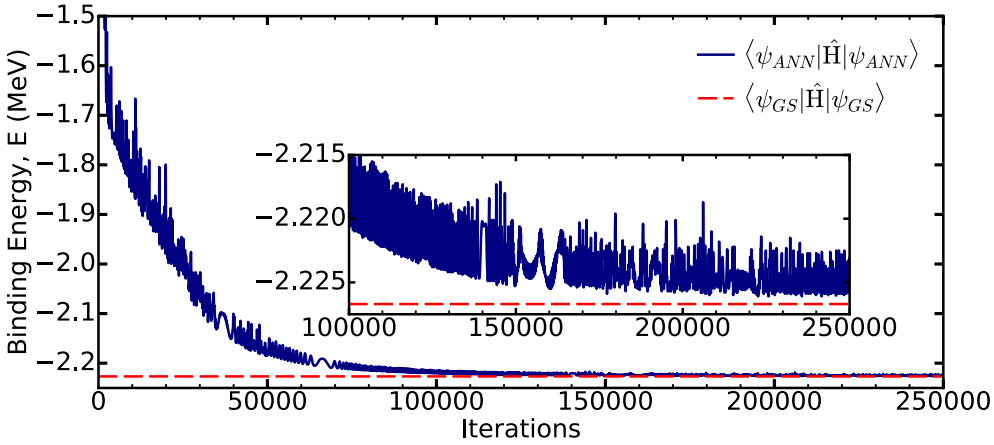

NUCLEAR PAIRING MODEL

We are exploring the solution of the many-body problem in the occupation-number formalism. As a prototypal example, we consider a simplified pairing model

$$H = \sum_{p,\sigma} d_p a^\dagger_{p\sigma} a_{p\sigma} + \sum_{pq} g_{pq} a^\dagger_{p\uparrow} a^\dagger_{p\downarrow} a_{q\downarrow} a_{q\uparrow} \quad \longleftrightarrow \quad d_p = p \;\; ; \;\; g_{pq} = g$$

- The Jordan-Wigner transformations map the Hamiltonian into the spin basis;
- We solve it using ANN ansatz and compare with exact diagonalization;
- The algorithm scales as the number of single-particle states squared;

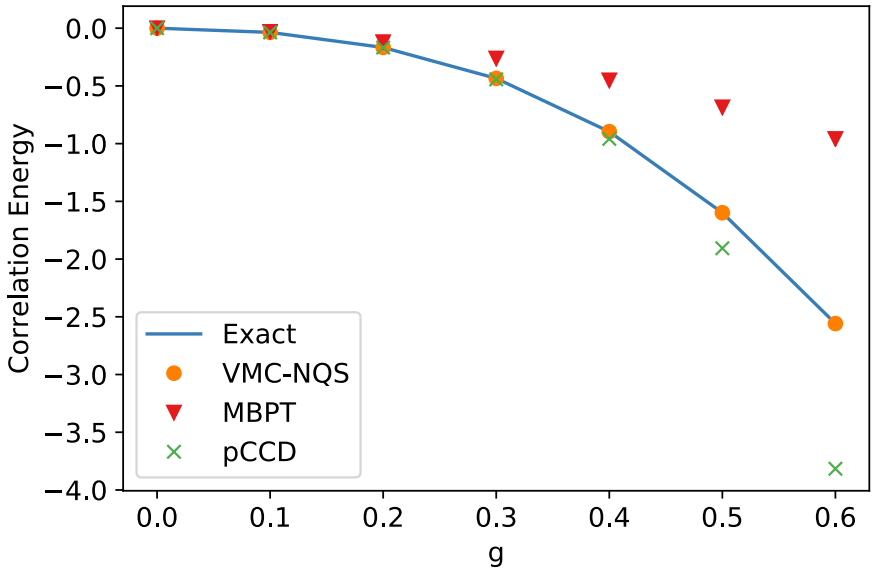

*M. Rigo, B. Hall, AL, Phys. Rev.E **107** (2023) 2, 025310*

CONFIGURATION-INTERACTION

The exact ground-state wave function can be expressed as a sum of Slater determinants

$$\Psi_0(x_1,\ldots,x_A) = \sum_n c_n \Phi_n(x_1,\ldots,x_A)$$

The occupation-number representation automatically encompasses fermion antisymmetry

$$|\Psi_0\rangle = \sum_{h_1\ldots,p_1\ldots} c^{p_1\cdots}_{h_1\ldots} |\Phi^{p_1\cdots}_{h_1\ldots}\rangle$$

$$|\Phi^{p_1\cdots}_{h_1\ldots}\rangle = a^\dagger_{p_1}\ldots a_{h_1}\ldots|\Phi_0\rangle$$

The dimensionality explodes quickly

$$\binom{N}{A} = \frac{N!}{(N-A)!A!}$$

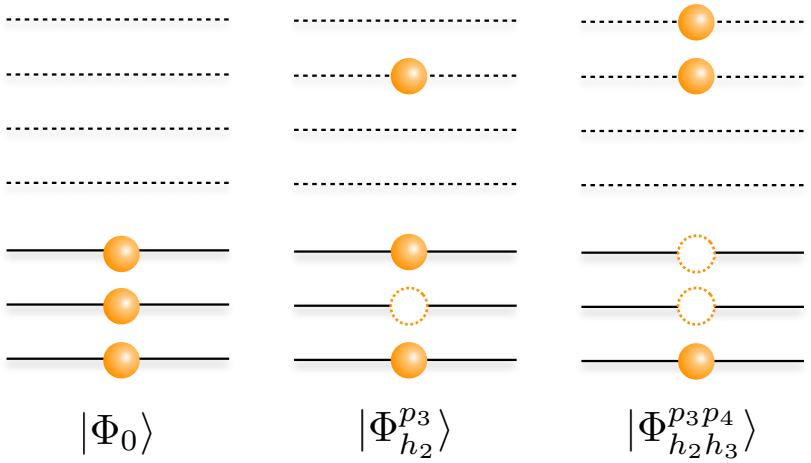

CONTINUUM QUANTUM MONTE CARLO

The trial wave function can be expanded in the set of the Hamiltonian eigenstates

$$|\Psi_T\rangle = \sum_n c_n |\Psi_n\rangle \qquad H|\Psi_n\rangle = E_n|\Psi_n\rangle$$

GFMC relies on imaginary-time propagation

$$\lim_{\tau\to\infty} e^{-(H-E_0)\tau}|\Psi_T\rangle = c_0|\Psi_0\rangle$$

*J. Carlson Phys. Rev. C **36**, 2026 (1987)*

GFMC suffers from the fermion-sign problem, but it is “virtually exact” for light nuclear systems.